

BAYESIAN OPTIMIZATION OF CATALYSTS WITH IN-CONTEXT LEARNING

A PREPRINT

 **Mayk Caldas Ramos**

Department of Chemical Engineering
University of Rochester
mcaldasr@ur.rochester.edu

 **Shane S. Michtav**

Department of Chemical Engineering
University of Rochester
smichtav@che.rochester.edu

 **Marc D. Porosoff**

Department of Chemical Engineering
University of Rochester
marc.porosoff@rochester.edu

 **Andrew D. White***

Department of Chemical Engineering
University of Rochester
andrew.white@rochester.edu

April 12, 2023

ABSTRACT

Large language models (LLMs) are able to do accurate classification with zero or only a few examples (in-context learning). We show a prompting system that enables regression with uncertainty for in-context learning with frozen LLMs (GPT-3, GPT-3.5, and GPT-4), allowing predictions without features or architecture tuning. By incorporating uncertainty, our approach enables Bayesian optimization for catalyst or molecule optimization using natural language, eliminating the need for training or simulation. Here, we performed the optimization using the synthesis procedure of catalysts to predict properties. Working with natural language mitigates the challenges of synthesizability since the literal synthesis procedure is the model’s input. We show that in-context learning improves past a model context window (maximum number of tokens the model can process at once) as data is gathered via example selection, allowing the model to scale better. Although our method does not outperform all baselines, it requires zero training, feature selection, and minimal computing while maintaining satisfactory performance. We also find Gaussian Process Regression on text embeddings is strong at Bayesian optimization. The code is available in our GitHub repository: <https://github.com/ur-whitelab/BO-LIFT>.

Keywords Bayesian Optimization, large language model, in-context learning, catalysis, materials design, AI

1 Introduction

Large language models (LLMs) are revolutionizing a wide range of domains across various fields of knowledge. While their most prominent applications lie in computational areas (such as natural language processing[1], text translation, classification[2–4] and summarization[5], question answering[6], sentiment analysis[7], code generation[8–10]), LLMs have also made significant contributions in diverse areas including legal analysis[11], biomedical research[12], finance[13], education[14, 15], social sciences[16], medicine[17], and entertainment[18–20].

In chemistry, LLMs have been employed to support research efforts in the areas of material design[21–24], reaction design[25, 26] and prediction[27–30], property prediction[31–34], and drug design[35–37]. Most of these applications are based on training a model using the transformer[38] architecture on a specific dataset. Recent advances have also led to the development of pre-trained models like the generative pre-trained transformer (GPT)[39] that are task-agnostic models capable of learning from a few examples shown to the model during inference time, termed in-context learning

*Corresponding author

(ICL)[40]. These models can even perform classification, and to a lesser extent regression, from tabular data, without needing any changes to their architecture or training methods[41].

Jablonka et al. [34] recently showed that it is possible to predict material and chemical properties with decoder-only models like GPT-3[40] using Language-Interfaced Fine-Tuning (LIFT)[41]. LIFT is the process of converting features and labels into a complete sentence, followed by fine-tuning. For example, using mapped experimental conditions "Oxidative coupling of methane using Mn-Na₂WO₄/ZSM-5 was ran at 750 C, with a total reactant flow rate of 20 mL/min (Ar: 8.0 mL/min, CH₄: 8.0 mL/min, O₂: 4.0 mL/min). The resultant C₂ yield is 4.81 percent" as a training example and at inference, "Oxidative coupling of methane using Co-Na₂WO₄/SiO₂ was ran at 775 C, with a total reactant flow rate of 20 mL/min (Ar: 3.0 mL/min, CH₄: 12.8 mL/min, O₂: 4.3 mL/min). The resultant C₂ yield is " will be prompted for completion." An overview of this process and our prompts is shown in Figure 1.

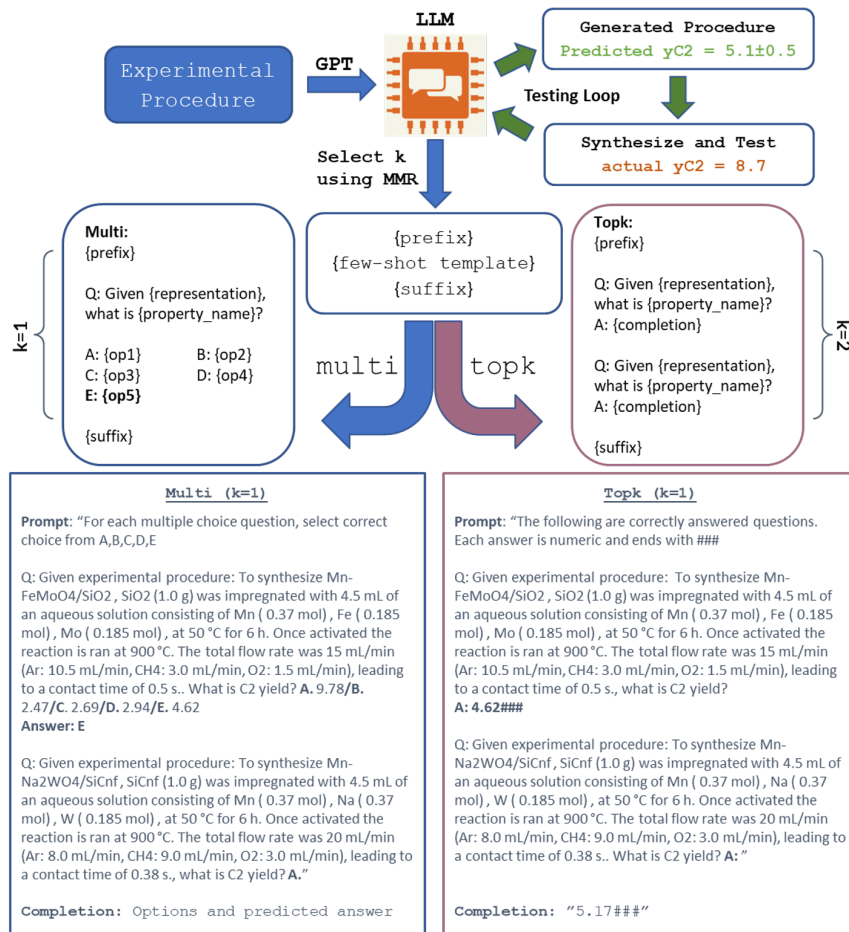


Figure 1: Our approach uses a Language-Interfaced Fine-Tuning (LIFT) framework with a Generative Pre-trained Transformer (GPT) to generate tokens that represent the reaction conditions that include a synthesis procedure. The catalyst synthesis and testing data is converted to an embedding vector and mapped to an objective function, *e.g.* C₂ yield. We create prompts involving multiple-choice options ("Multi", left panel) and single context completions ("Topk", right panel). In this scheme, multi selects only one example ($k = 1$) from the list, while topk selects two. The prompt starts with an instruction to the LLM of what the generated completion should resemble. Following this, the formatted examples for in-context learning are created. While multi generates five alternatives around the label, topk only uses the label. Finally, the sequence for which the model should respond is added to both prompts. The two lower panels show actual prompts generated by using Multi (left panel) and Topk (right panel) templates. Both examples illustrate the string to the LLM when selecting $k = 1$ to create the prompt. For multi, the model generates all five options, whereas for topk the model only generates the numerical value of the prediction.

ICL is prefixing the prompt with examples to "train" without actually modifying the LLM parameters[40]. ICL has been found to be less accurate than fine-tuning for LIFT-style regression or classification of materials and molecules[34]. Our

goal in this paper is to obtain prediction uncertainty from the LLM to optimize materials and molecules using Bayesian optimization (BO), which is iterative cycles of training and proposing new points to label[42]. ICL is preferred because it simply requires changing the prompt at each iteration, but limited context windows of the underlying LLM prevent ICL from being directly applied past a certain training amount.

The main contributions of our work are to show: (1) ICL can scale and improve accuracy up to 1,000s of examples by context selection; (2) regression with uncertainty is possible via token scores and prompts; (3) uncertainties enable BO to design catalysts and reaction conditions.

To evaluate our methodology, we employed it for predicting two properties: aqueous solubility of drug-like molecules and reaction yield. Specifically, we used the ESOL dataset[43] and catalyst dataset for oxidative coupling of methane derived from the work of Nguyen *et al.*[44].

Designing new catalysts is a critical challenge to address climate change. About one-third of the global gross domestic product (GDP) relies on catalytic processes to produce value-added chemicals and fuels from fossil-based resources[45]. One of the main challenges is navigating the complex experimental space to identify materials capable of converting carbon-neutral or negative feed stocks into value-added products.[46–48] Here we represent catalysts with the natural language used in their synthesis recipes, which makes zero assumptions about catalyst structure and mechanism, with implicit synthesizability embedded into the experiments proposed by the model. The way we represent materials is obviously critical for the ability to predict properties and is challenging in complex materials, such as inorganic zeolites.[49, 50]. The idea of using natural language has been explored in predicting materials properties, where the materials description is embedded into a vector via a model trained with unsupervised learning [1, 21, 51, 52]. In contrast, we are using decoder-only models – the LLMs are directly predicting the catalyst property from reaction conditions and synthesis procedures. Such decoder-only models are highly sought after in catalysis, because they can also be used to do inverse design and suggest an actionable experiment[24].

Aqueous solubility is a fundamental physicochemical property of chemical compounds, defined as the maximum concentration of a solute that can dissolve in water at a given temperature and pressure.[53] It plays a crucial role in various fields, including drug design, environmental studies, and chemical engineering [54–58]. Accurate prediction of solubility is essential for the development of efficient pharmaceuticals, understanding the fate of chemicals in the environment, and optimizing industrial processes. However, its accurate prediction remains a challenge.[59, 60] Traditional methods for predicting solubility have been based on experimental measurements, quantitative structure-activity relationships (QSAR), and molecular simulations[61, 62]. However, these approaches can be time-consuming, expensive, and sometimes inaccurate, especially for large and diverse sets of compounds[63]. In this context, LLMs have shown promising results in predicting chemical properties, reaction outcomes, and synthesizability[25–27, 34].

There has been much more work in exploring language in the related fields of molecules and bio-macromolecules[21–23, 28–30, 34, 64, 65]. Specifically, the use of pre-trained LLMs with Bayesian optimization has been done in Yang *et al.* [66]. In chemistry, Frey *et al.* [67] have explored using decoder-only GPT models for molecular design. There has also been multiple encoder-decoder models as well, which can produce novel compounds and be used to do fine-tuning for property predictions[68–70]. However, there is to our knowledge no work on regression with ICL and Bayesian optimization.

There has been recent work exploring what is possible with ICL, and improving its accuracy. ICL[40] combined with chain of thought techniques[71–73] or symbolic tools (e.g., programming languages) has been explored for improving accuracy[74, 75]. The order and identity of the examples are important[76] and can be arranged. Dai *et al.* [77] also showed that ICL may be viewed as a kind of gradient-descent like process.

2 Methods

IUPAC names of molecules were used to predict aqueous solubility (from ESOL[43] dataset), and natural language descriptions of synthesis procedures were used to predict C_2 yield for oxidative coupling of methane ($2CH_4 + O_2 \rightarrow C_2H_4 + 2H_2O$). Nguyen *et al.*[44] evaluated 12,708 different experimental configurations for a range of parameters, including catalyst composition, temperature, and flow rate. The conditions were converted to natural language with the following prompt: “Given {x}, what is {property_name}?” An example prompt for querying the C_2 yield of the reaction is “To synthesize Mn-Na₂WO₄/BN, BN (1.0 g) was impregnated with 4.5 mL of an aqueous solution consisting of Mn (0.37 mol), Na (0.37 mol), W (0.185 mol), at 50 °C for 6 h. Once activated the reaction is ran at 900 °C. The total flow rate was 20 mL/min (Ar: 14.0 mL/min, CH₄: 4.8 mL/min, O₂: 1.2 mL/min), leading to a contact time of 0.38 s.”

BO of materials can be reviewed in Shahriari *et al.* [78], Liang *et al.* [79], Baird *et al.* [80], and Valletti *et al.* [81]. BO is a black-box optimization method where we seek to maximize a function that is expensive, noisy and/or has unknown analytical form.[82] By incorporating uncertainty information, BO guides the exploration-exploitation trade-

off, selecting the most informative points for evaluating the true objective function.[83] Consequently, it enables a more efficient search for optimal materials and chemical systems, minimizing the number of expensive experimental evaluations required [84]. In the case of our two problems, we are trying to maximize C₂ yield and solubility. BO reduces the amount of experimental conditions and catalysts synthesis needed to optimize yield[85]. BO requires uncertainty in model predictions, usually achieved via Gaussian process regression (GPR)[42].

We used LangChain[86] to call the GPT-3[40] and the GPT-4 [87] models, trained and maintained by the OpenAI company. We apply the LIFT[41] approach to create the prompts to be fed into the LLMs (see Figure 1). In the LIFT procedure, features are incorporated into natural language sequences to allow LLM to address non-language downstream tasks. To do ICL, we prefix previous examples. To enable ICL beyond a few examples, instead of prefixing all examples, we down-sample our in-context examples to solve the problem of ICL past the LLM context window using max marginal relevance (MMR) selection[88, 89]. MMR combines the search for the most similar examples to a specific sequence while maximizing diversity. We compute similarity via Euclidean distance between Ada embeddings[90]. Given the features (prompt) that we want to predict, we find the most relevant examples and prefix them at inference time. This prompt creation procedure is implemented in LangChain[86] using the FAISS library[91] and Ada-002 embeddings[90].

We do regression with uncertainty by using token probabilities, similar to the action selection process used in Ahn et al. [92] (Figure 1). To get uncertainty, we devised two prompting strategies: (i) multiple choice option template and (ii) Top k completions template. Those templates are referred to as “multi” and “topk” throughout this study. The rationale for multi was that only a single token (the option letter) indicated the choice so that the probability of that one token could succinctly give a range of choices. Topk requires generating k completions and then the logprobs of the entire completion are marginalized to compare. This produces discrete probability distributions, which can then be used directly with acquisition functions for BO[42]. Finally, these two methods are combined into a BO loop for optimizing catalysts and reaction conditions. This is advantageous because the BO approach requires no training with minimal computing required for LLM inference.

Figure 1 illustrates how each template is constructed by selecting $k = 1$ examples as context. Both templates follow the same general prompt structure: “{prefix}{few-shot template}{suffix}”. The {prefix} gives context on how the structure of the LLM’s response to avoid hallucinations. {few-shot template} creates the context by concatenating k examples using the following structure: “Given {representation}. What is {property_name}? {completion}”. Since the {prefix} is fixed and the {suffix} uses the same structure: “Given {representation}. What is {property_name}?”, multi and topk differ on how they build {completion}. When using multi, five options (A, B, C, D, and E) are considered. We used five options because that is the number of token probabilities returned in the OpenAI API. The correct label is randomly placed as one option, and the four options are filled via sampling from $y \times s$, $s \sim \mathcal{N}(1, 0.1)$, where \mathcal{N} is a normal distribution.

Examples of prompts created using each template are shown in the bottom panels of Figure 1. Hence, the LLM completes all five alternatives, generating five possible completions. On the other hand, topk simply uses the label as {completion}, and then it requests generating $n = 5$ completions. For “chat” type models (e.g., GPT-4), logprobs are not provided and we weight each completion as equally probable – a strong limitation.

The above prompting creates a discrete probability distribution. The completions are converted into real numbers and their associated probabilities describe the distribution. The usual BO acquisition functions expected improvement (EI), and upper confidence bound (UCB) can be reformulated for discrete distributions. EI, $u_{ei}(x)$, balances exploration and exploitation and is defined for discrete probability distributions as follows:

$$u_{ei}(x) = \text{E}[\max(0, y^* - y_i)] = \sum p_i \max(0, y^* - y_i) \quad (1)$$

Where p_i, y_i are the pairs of predicted values/probabilities at x using the model and y^* is the maximum known measured y value. The other acquisition functions can be similarly defined.

Sometimes we observe only one value from topk because the additional completions differ in a whitespace token, punctuation, or number formatting. When this occurs, we replace the discrete distribution with a normal distribution centered at the value with a standard deviation equal to the sample standard deviation of all y_i in training data.

For our baselines, we employed LIFT (fine-tuning), Kernel Ridge Regression[93] (KRR), Gaussian Process Regressor[94] (GPR), and k-Nearest Neighbors[95] (KNN). LIFT, based on the text-ada-001 model, utilized the topk template and was trained for eight epochs with a learning rate multiplier of 0.02, following the parameters established by Jablonka et al. [34]. For KRR, we embedded the prompts generated by the topk approach using the text-embedding-ada-002 model. Both the embedded input and the labels were normalized during the training, and we employed a regularization strength of $\alpha = 0.5$. In contrast, we trained GPR using three types of inputs: (1) LIFT

prompts embedded with the "text-embedding-ada-002" model, (2) the same prompt using the Material BERT [21] model, and (3) the numerical features vector employed in crafting the natural language prompts. Due to the high dimensionality of these embeddings (e.g., 1536 dimensions for the ada embeddings), training GPR models with a large number of data points proved to be computationally challenging. To avoid these limitations, we applied isometric mapping with 32 components for dimensionality reduction[96], facilitating more efficient model training for GPR. Lastly, we implemented KNN using the `SemanticSimilarityExampleSelector` from the LangChain [86] library. In this work, we focused on only $k = 1$ nearest neighbor for our analysis.

The ICL and the GPR baseline model predict uncertainty and are used as surrogate models in BO[79, 97]. Unless otherwise stated, all examples are with a finite pool of data and the goal of the Bayesian optimization is to find the point with the maximum label. We implemented an *ask-tell* interface for our methods. Firstly, a random example is taken from the pool of possible elements. This example is used to initialize the ICL or GPR model. Since fine-tuning takes significant GPU resources and time, it is infeasible to fine-tune repeatedly throughout the BO. For that reason, we did not use the fine-tuned models as surrogate models. Secondly, the model goes through repeated ask (finding the pool member that maximizes $u(x)$) and tells (labeling the point chosen). To increase efficiency, rather than evaluate all pool members on the acquisition function, we used a Hyde[98] like strategy of inversely designing predicting a hypothetical \hat{x} from $1.5 \times y^*$ (a point 50% larger than current maximum) by inverting the prompts. This \hat{x} is then used with above prompt selection strategy to choose 16 pool examples.

All Bayesian optimization plots show y_N^* – the current best at sample count N . The random baseline was estimated via a quantiling of the datapoints. Namely, for random sampling y_N^* is estimated with:

$$E[y_N^*] = \sum_i^K y_i \mathbf{P}(s_m = y_i) ; s_m = \max(y_1, y_2, \dots, y_N) \quad (2)$$

$$\approx \sum_j^Q (j^N - (j-1)^N) \left(\frac{1}{Q}\right)^N q_j$$

where q_i is the i th quantile of y (out of Q) and K is the number of datapoints in the pool.

The datasets are divided into training/test groups using a split of 80/20. The ICL model can select from all training examples and the training data is used for the LIFT/GPR training.

Unless otherwise stated, we use the `text-curie-001` model for hyperparameter selection, which has only 6.7B parameters[40] due to the cost and time of larger models. We did experiments up to GPT-4[87] on select tasks and observed consistent improvement. Thus, we expect our conclusions about comparing prompting strategies and datasets to hold for `text-curie-001` and above.

3 Results and discussion

First we consider the effect of available examples on ICL in Figure 2. At zero shot ($N = 0$) the model is relying on potential pre-training on the tasks. The difference between topk and multi prompts in zero-shot is the prefix prompt that explicitly specifies the desired format for predictions. Zero-shot did poorly. For the solubility data, only the multi method produced valid responses, though the accuracy of these predictions was poor. The ESOL[43] dataset, published in 2004, has since served as a benchmark for solubility models; however, despite potential contamination there was poor zero-shot accuracy. The C_2 dataset generated constant values for each prompt (refer to the initial panel in Figures A.13 and A.16). The C_2 dataset was published after `text-curie-001` training, and thus cannot be part of the model’s pre-training data.

The model can choose data from N training points to create context, but only with k examples. As k increases from 1 to 10, improvements in mean absolute error (MAE) and Pearson correlation (r) can be observed, with subtle differences between the multi and topk methods. Parity plots are in Figures A.3 and A.6. However, we kept k at 5 due to the large context window required for C_2 results.

When $N > k$, examples were selected using the max marginal relevance[89] as implemented in LangChain[86]. This gives the ability to improve accuracy beyond $N = k$, as shown in Figure 2. Parity plots are shown in Figures A.2 and A.5. The multi method exhibits a stronger dependence on the number of points, indicating its larger sensitivity to the examples chosen for context creation and a reduced ability to leverage pre-training information. Using `text-curie-001` with topk prompt shows good results in a low-data regime, with an MAE of ~ 1.1 and a correlation of ~ 0.6 with few data points. In comparison, using multi requires ~ 500 data points to reach similar performance.

The nearest neighbor prediction (KNN) baseline shows how much accuracy comes from just choosing the closest example (via text embeddings). The kernel ridge regression (KRR) baseline shows how much accuracy comes from averaging around nearby examples. The conclusions from Figure 2 are topk is better than multi, ICL is less accurate than trained baselines relying on text embeddings, and ICL has good likelihoods – meaning they are suited to Bayesian Optimization.

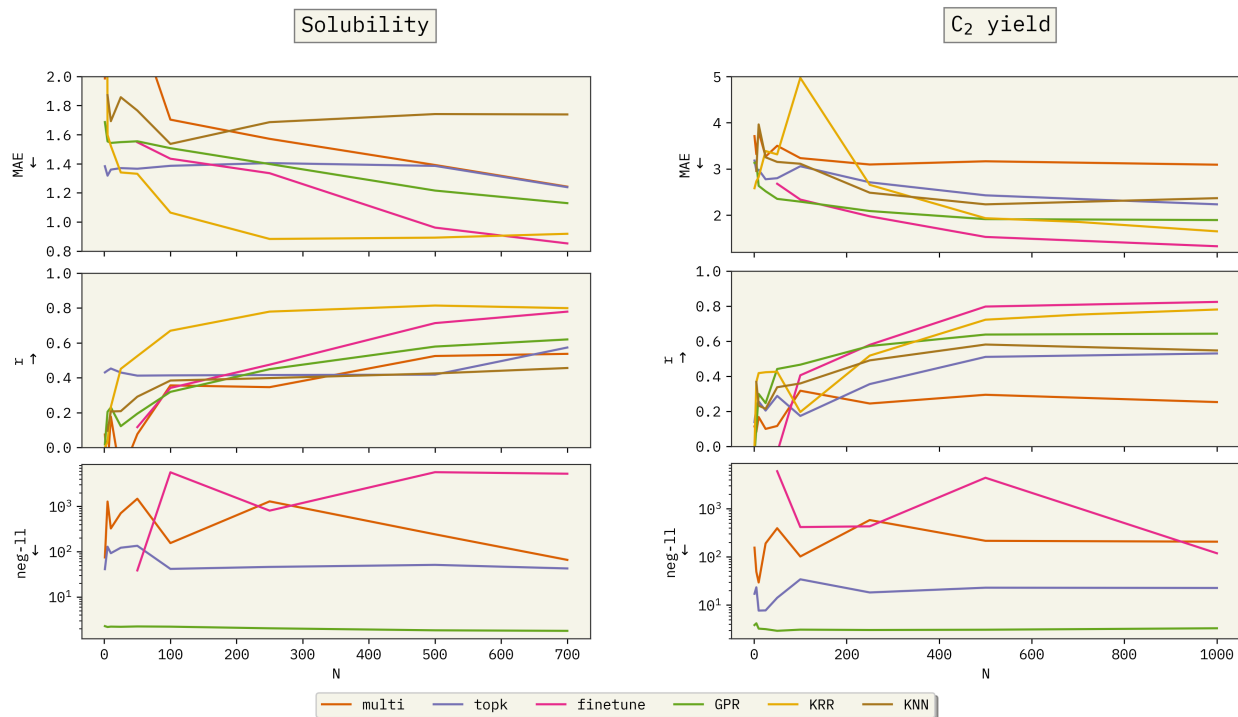


Figure 2: Dependence of the six models considered in this work as a function of the number of training points N from where the model could select examples to create the context (for ICL models) or to train (for baseline models). In these experiments, our ICL models have a fixed example selector size of $k = 5$, temperature of $T = 1.0$, and used the `text-curie-001` model. The negative log-likelihood (neg-ll) does not follow a trend on changes in N despite the improvement in the other metrics. The arrows in y-axes indicate the direction of improvement. The results show that using in-context learning (ICL) is enough to be comparable to the fine-tuned model for the solubility dataset.

The C_2 yield dataset was assembled from text and tables from Nguyen et al. [44] and could not have been in any pre-training data from the models considered here. The C_2 dataset exhibits greater complexity than solubility data, as it contains natural language descriptions of catalyst synthesis processes instead of explicit molecular representations. The experimental measurements in the C_2 dataset also likely have larger error because catalysts are both synthesized and tested in a high throughput apparatus, potentially leading to the lower accuracy. Among both examples, topk gave good likelihoods but relatively poor correlation or standard deviations. Parity plots for all experiments can be found in Figures A.13 and A.16.

Analogous to solubility dataset, both multi and topk methods benefited from increasing the number of training points N . However, as illustrated in Figure 2, performance appears to plateau and does not improve beyond $N = 200$ in this instance. Unlike the solubility dataset, we did not observe significant improvements as k or T values were increased in the C_2 dataset (See Figure A.11).

The ranking of model performance in the C_2 dataset is similar to the solubility dataset. However, the baselines performed significantly better. We hypothesize that the higher complexity of the C_2 dataset, along with the pronounced similarity between data points, made the `text-curie-001` model incapable of effectively learning from context alone. As a result, incorporating additional context may inadvertently distract the model and diminish the quality of its predictions. Figure A.11 provides a visual summary of our findings.

Figure 3 shows the effect of larger and more recent models for the C_2 catalyst dataset. Table 1 contains the hyperparameters used in each experiment depicted in Figure 3 (see Supporting Information for justification of hyperparameters). Specifically, we provided $N = 1000$ training points to the model and constructed a context with a size of $k = 5$. The

text-curie-001 model, which was trained using data collected up to October 2019, yielded an MAE of 2.333 and a correlation of 0.530. In contrast, the more recent gpt-4 model, resulted in an MAE of 1.854 and a correlation of 0.613. The observed enhancement in performance from text-curie-001 to gpt-4 cannot be attributed to contamination in the training set, as C₂ is first assembled in this work. Instead, it is likely associated with the multi-benchmark continued improvement in accuracy with model size[99]. Figure 3 also display parity plots for KNN, KRR, and finetune. GPT-4 outperformed the KNN baseline, which had an MAE of 2.366 and a correlation of 0.547, but not all baselines. Although GPT-4 has better performance, it has no logprobs and thus we assign equal probability to all outputs. Thus, we continued to use text-davinci-003 in our analysis.

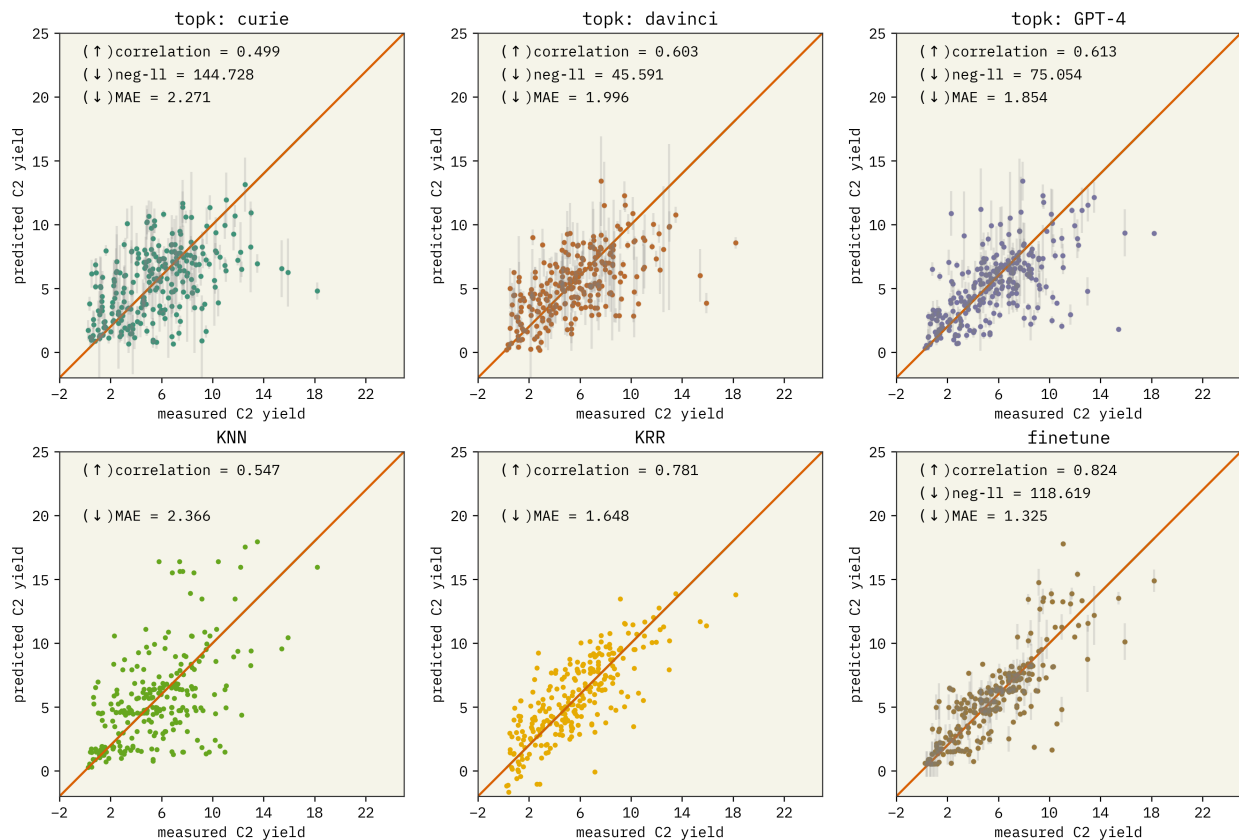


Figure 3: Parity plots with uncalibrated uncertainties comparing the performance of different large language models (LLM) evaluated on the C₂ yield dataset. In the first row, from left to right, we show our results for the topk approach employing the following LLMs: text-curie-001, text-davinci-003, and gpt-4. We can observe that the predictions improved over time as newer models were released. In the second row, we show the results for our baselines: nearest neighbor (KNN), kernel ridge regression (KRR), and fine-tuning using text-ada-001 as base model. Notably, curie struggled to learn from the context for the C₂ dataset. Nevertheless, GPT-4’s results are comparable to those of KRR. Hyperparameters are available in Table 1.

The models were found to be over-confident in their calibration [100, 101]. For some data points, the language models predicted only one value with logprobs equal to 1.0. The standard deviation of the training data population was substituted for these examples. We recalibrated the models by introducing an uncertainty scaling factor expected to minimize the miscalibration area associated with each model via the optimize_recalibration_ratio from the Uncertainty-Toolbox[101, 102] as shown in Figure A.22.

Figure 4 displays the parity plots after recalibration for the text-davinci-003 and gpt-4 models, as well as the baselines for which uncertainties could be computed. Remarkably, ICL outperforms all considered baselines (see the first row in Figure 4 and Table A.1) — with the additional benefit of not requiring a supervised training process, which can be time-consuming and expensive. Table A.1 presents the metrics obtained in this study and compares them with state-of-the-art (SOTA) models. SOTA models consist of transformers that have been specifically trained for the solubility dataset. We showed that a considerably simpler process — prompt engineering to create the context for ICL

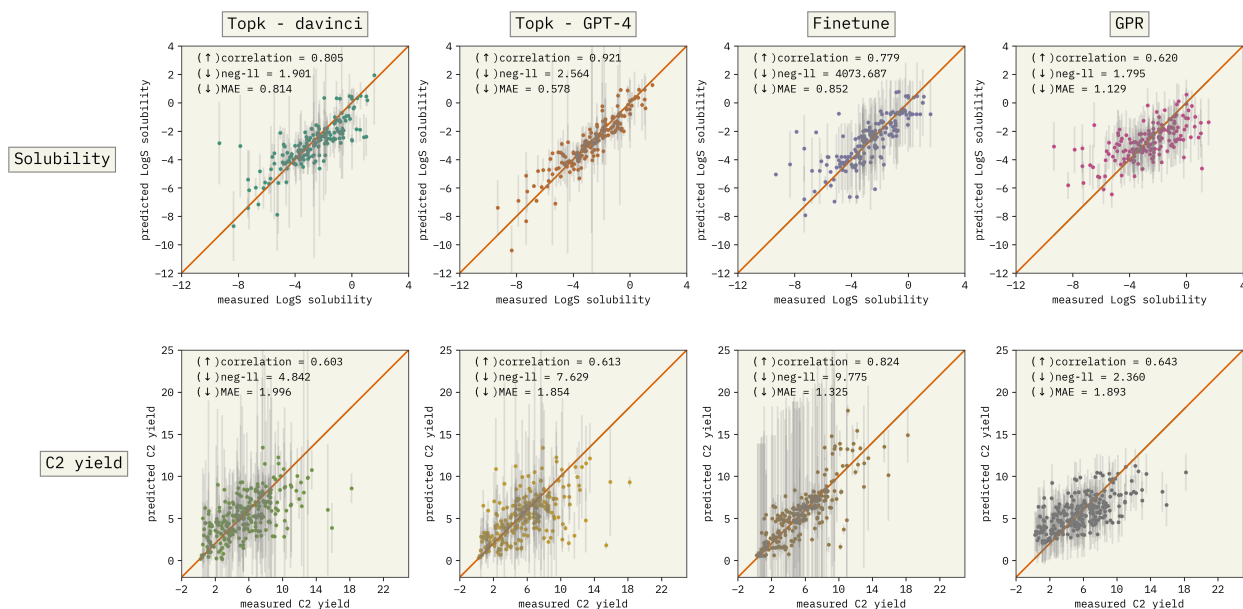


Figure 4: Parity plots with recalibrated uncertainties comparing the performance of in-context learning (ICL), fine-tuning, and training a Gaussian Process Regressor (GPR) for solubility and C_2 yield datasets. We observe that ICL outperformed the baselines considered in this work for the solubility dataset. However, for the C_2 yield dataset, ICL obtained a performance comparable to GPR but was unable to outperform the fine-tuned model.

— could yield comparable performance. On the other hand, ICL could not surpass fine-tuning in the C_2 dataset (refer to the second row in Figure 4). ICL cannot provide sufficient context for the model to effectively learn the complexities of the C_2 yield dataset. Furthermore, the prompts are larger in this case, and we could not increase the context size to enhance performance. Nevertheless, ICL models still demonstrated performance comparable to that of GPR.

model	prompt	RMSE ↓	MAE ↓	r ↑	neg-ll ↓
text-curie-001	multi	13.487	3.878	0.051	8.139
text-curie-001	topk	3.016	2.271	0.499	16.985
text-davinci-003	multi	3.615	2.576	0.411	15.031
text-davinci-003	topk	2.652	1.996	0.603	4.842
gpt-4	topk	2.683	1.854	0.613	7.629
Fine-tuned text-ada-001	topk	1.936	1.325	0.824	9.775
Kernel Ridge Regression (KRR)	topk	2.114	1.648	0.781	-
Nearest Neighbor (KNN)	topk	3.247	2.366	0.547	-
GPR with ada embeddings	topk	4.173	1.573	0.774	3.160
GPR with MatBERT embeddings	-	5.303	1.786	0.741	2.776
GPR with numerical feature vector	-	4.913	1.722	0.738	3.351

Table 1: Performance metrics associated with predictions on the C_2 dataset with optimal values highlighted in bold. Displayed models represent instances for each model type using the hyperparameters selected by the study varying each parameter. For all LLMs, we defined temperature $T = 0.7$, context size $k = 5$, and $N = 1000$ training points. All baselines were trained also considering $N = 1000$ training points. Displayed metrics were calculated after recalibration.

3.1 Bayesian Optimization

After evaluating the models’ performance in regression tasks, we did Bayesian optimization to maximize LogS solubility and the C_2 yield. The expected maximum of randomly sampling sequence of values was analytically calculated (refer to Section 2) and used as a baseline for the BO experiments. Fine-tuning for each iteration is impractical, since it requires hours of compute at each iteration. Therefore, LIFT was not included in the BO experiments. An ask-tell interface was used to examine a pool of samples, select the subsequent sample based on an acquisition function, and provide that point to the model with the respective label. These points contributed to constructing the context for future predictions

in ICL or training the GPR model. Five independent trials were carried out for each model, and the average results were computed (Figure 5). Faded lines represent individual trials. Each BO run was started with 100 training data points. The initial training data is used to compute the scaling factor to recalibrate the predicted uncertainty that was used in the BO run.

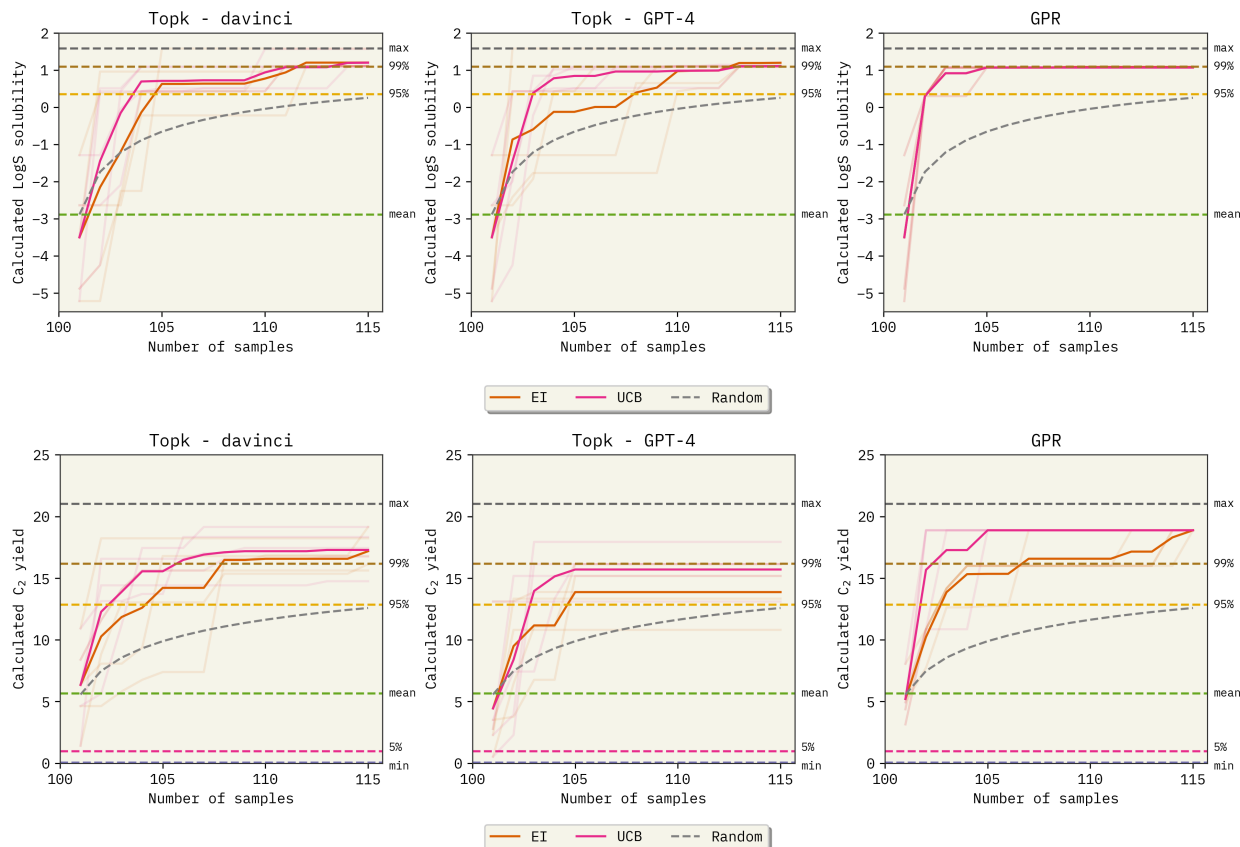


Figure 5: Bayesian optimization (BO) history. We implemented BO using an ask-tell interface. At each new sample, we plotted the maximum label found up to that point. Initially, 100 points were fed to the model to compute the scaling factor to calibrate uncertainty predictions. We employed expected improvement (EI) and upper confidence bound (UCB) as acquisition functions. Experiments with greedy and probability of improvement were also conducted, but we observed that the results do not strongly depend on the acquisition function. The curve labeled “Random” illustrates the expected value of the distribution $S = \max(y_0, y_1, y_2, \dots, y_N)$ for a sequence of size N , representing the scenario where N samples are selected randomly. Optimizing on the solubility dataset outperforms random selection and the GPR baseline, reaching the 99% percentile and identifying the maximum in one of the five replicates. On the other hand, the C_2 dataset exhibits increased complexity. Therefore, although in-context learning (ICL) reached the 99% percentile after 15 samples, it failed to locate the maximum value within the pool. It is noteworthy that GPR, while also unable to find the maximum, approached it more closely.

Figure 5 is the progression of BO. Each curve starts from a randomly chosen sample (the same sample was selected for each model in every run to minimize its effect on comparisons). The curves are the maximum value identified up to that point. All models reached the 95% percentile solubility around 5 examples in BO. Notably, both `text-davinci-003` and `gpt-4` converged to the same maximum value after labeling 15 new samples (beyond initial 100). On average, a maximum of ~ 1.2 logS was identified. This value is lower than only three other values in a pool of 882 molecules. Individually, `text-davinci-003` found maximum values of LogS 1.11, 1.58, 1.11, 1.11, and 1.11, `gpt-4` obtained 1.12, 1.58, 1.09, 1.09, and 1.11. Both models could identify the maximum (1.58) in at least one of the five replicates. These experiments did not strongly depend on the acquisition functions. Training the GPR model with additional samples (beyond the initial 100) did not improve our experiments. The left panel in Figure 6 illustrates the histogram of the solubility dataset, with the average values procured for each model, represented as vertical lines.

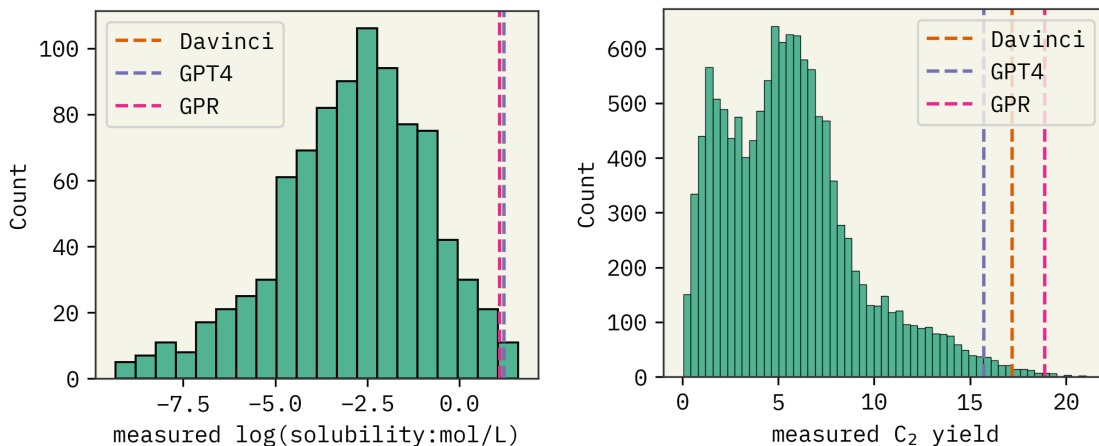


Figure 6: Histograms illustrating the data distribution for the solubility dataset (left panel) and the C_2 dataset (right panel). Dashed lines indicate the mean of 5 BO runs identified by each model during the BO process, utilizing the expected improvement acquisition function. Although `gpt-4` and `text-davinci-003` outperform GPR in the solubility dataset, their performance in the C_2 dataset is slightly inferior in comparison to GPR.

C_2 showed better performance for GPR with text embeddings than ICL. The ICL models reached the 99th percentile after 15 samples, but their performance did not improve substantially after that. Surprisingly, while `text-davinci-003` managed to capture some of the top 66 values in the dataset, `gpt-4` was only successful in reaching the top 180. This may be because of the lack of token probabilities in `gpt-4`, since OpenAI does not expose logprobs for chat models. GPR managed to identify the 18th-best example from a pool of 12,708 procedures.

We demonstrated that BO using ICL is feasible in low-data regimes. For the solubility dataset, both `text-davinci-003` and `gpt-4` using `topk` outperformed GPR. However, although it did not outperform GPR in our experiments in the C_2 yield dataset, we should note that we restricted the number of examples used in the context to mitigate expenses — which could decrease performance — and that LLMs are continuously being enhanced, as discussed earlier. The GPR baseline presented here is also novel to the best of our knowledge, and provides a compelling approach. ICL still may be preferred because it does not require training, can be used for inverse design, and will see continued improvement.

3.2 Inverse design

We employed our approach to achieve the inverse design of experimental procedures, building upon the study conducted by Jablonska *et al.*[34]. For inverse design, we utilized the same ICL concept discussed in previous sections of this work. The prompt for direct prediction was structured as: “Given {representation}. What is {property_name}? {completion}”, which was used to generate the context. A similar structure was used as a suffix to the prompt, removing the {completion} field. Conversely, the inverse design involved reversing the prompt order and requesting the LLM to complete the following prompt structure: “If {property_name} is {property_value}, then {representation} is {completion}”.

To explore inverse design, we considered an in-house dataset[103] of CO yield over tungsten carbide catalysts for the reverse water-gas shift reaction ($\text{CO}_2 + \text{H}_2 \leftrightarrow \text{CO} + \text{H}_2\text{O}$). CO yield was experimentally measured for 37 configurations that varied a dopant metal and concentration, tungsten loading, carburization temperature and reaction temperature. We adopted two approaches to predict which experimental procedure should be tested next in the laboratory: (1) feeding all 37 data points to the model and subsequently using the model to select the optimal experiment from a pool of 2158 synthetic data points, and (2) employing the inverse design prompt to inquire which tungsten carbide preparation procedure would result in a CO yield of 20%.

We applied `gpt-4` to both tasks. Through BO on the existing data, the following procedure was proposed to maximize the EI acquisition function with a CO yield of $19.93 \pm 0.69\%$: “A 15 wt% tungsten carbide catalyst was prepared with a Cu dopant metal at 5 wt% and carburized at 950°C. The reaction was run at 350°C.” We abbreviate this sample proposed by the EI function as 5Cu-WC(950). Alternatively, when asking `gpt-4` to generate an experimental procedure with a CO yield of 20% using ICL and the inverse prompt, it produced the following procedure: “Synthesis procedure: A 25 wt% tungsten carbide catalyst was prepared with an Ni dopant metal at 1.0 wt% and carburized at 900°C. The reaction was run at 375°C.” We abbreviate the sample proposed by ICL as 1Ni-WC(900).

For the 1Ni-WC(900) experiment at a reaction temperature of 375 °C predicted by ICL, we obtained a CO yield of 3.2%, which was also lower than expected. Upon inspecting the dataset in an attempt to interpret the prediction by ICL, we observe that the tungsten carbide pool includes three experiments over Ni-WC, two with Ni loading at 0.5 wt% and one with Ni loading of 0.25 wt%, all carburized at 835 °C. The highest CO yield of the Ni-based samples in the dataset is the 0.25Ni-WC(835) run at 350 °C, which reached 9.54%.

The Ni-based experiments are another important example that demonstrates the limitations of the BO technique for inverse design. Although CO is the desired product from reverse water-gas shift, there is a methanation side reaction that becomes more active with increasing temperature over the Ni-based catalysts as shown in Figure B.23. The CH₄ selectivity increases from 59% at 325 °C up to 84% at 375 °C, decreasing the CO yield from 4.7% to 3.2%, even though the CO₂ conversion increases from 11.9% to 22.7% over the same temperature interval. Because we classified the catalyst with CO yield, which is the product of CO₂ conversion and CO selectivity, the model likely could not distinguish between high conversion and CO selectivity and was therefore unable to predict the existence of the methanation side-reaction at elevated temperatures. Upon updating the model with the result of the 1Ni-WC(900) experiment, we anticipate it will become privy to the side reaction over Ni-based catalysts at elevated temperatures, and therefore, avoid the Ni dopant at high temperature in future iterations.

Looking back to the C₂ dataset from Nguyen *et al.*[44], it is possible that BO could not predict C₂ yields above 20% because the experiments were outliers or anomalies. Out of the 12,708 experiments, only 12 reach C₂ yields above 19%. Therefore, there is a distinct possibility that in a pool of 12,708 high throughput experiments, that at least 0.1% are outliers or contain significant measurement error. While inverse design using LLMs is possible, it remains crucial to validate the proposed experimental procedures in the lab to confirm their feasibility, accuracy and reproducibility.

4 Conclusion

We showed that using example selection for in-context learning (ICL) enables frozen Large language models (LLM) to learn past their context window size without retraining. The prompting approach developed in the current study enables LLMs to make predictions with uncertainties. Hence, techniques such Bayesian optimization (BO) which use uncertainties are used on the two datasets.

In this study, we explored the use of LLMs for downstream regression tasks in chemistry and materials. We applied our models to the prediction of LogS solubility data and C₂ yield in catalyst reactions. In addition, we carried out BO and inverse design for proposing new experimental procedures to synthesize innovative catalysts.

Using well-designed prompts to enable uncertainty prediction from LLMs is a powerful tool for techniques such as Bayesian optimization (BO). Despite the catalyst experimental space’s complexity, ICL-enabled BO performs comparably to BO using Gaussian Process Regression (GPR) with minimal samples. While for more simple prompts, such as the IUPAC names used in the solubility dataset, ICL outperformed GPR.

Additionally, LLMs are suitable for inverse design by inverting the prompt order, allowing them to propose new experimental procedures using ICL. LLMs can suggest new plausible experiments.

Acknowledgments

This research is supported by the National Science Foundation under Grant No. 1764415 and the National Institute of General Medical Sciences of the National Institutes of Health (NIH) under award number R35GM137966. The authors also thank the computational resource and structure provided by the Center for Integrated Research Computing (CIRC) at the University of Rochester.

References

- [1] Jacob Devlin, Ming-Wei Chang, Kenton Lee, and Kristina Toutanova. Bert: Pre-training of deep bidirectional transformers for language understanding. *arXiv preprint arXiv:1810.04805*, 2018.
- [2] Jibing Gong, Zhiyong Teng, Qi Teng, Hekai Zhang, Linfeng Du, Shuai Chen, Md Zakirul Alam Bhuiyan, Jianhua Li, Mingsheng Liu, and Hongyuan Ma. Hierarchical graph Transformer-Based deep learning model for Large-Scale Multi-Label text classification. *IEEE Access*, 8:30885–30896, 2020. ISSN 2169-3536. doi:10.1109/ACCESS.2020.2972751.
- [3] Ilias Chalkidis, Manos Fergadiotis, Sotiris Kotitsas, Prodromos Malakasiotis, Nikolaos Aletras, and Ion Androutsopoulos. An empirical study on Large-Scale Multi-Label text classification including few and Zero-Shot labels. October 2020.

- [4] Jiong Zhang, Wei-Cheng Chang, Hsiang-Fu Yu, and Inderjit Dhillon. Fast multi-resolution transformer fine-tuning for extreme multi-label text classification. *Adv. Neural Inf. Process. Syst.*, 34:7267–7280, 2021. ISSN 1049-5258.
- [5] Yang Liu and Mirella Lapata. Text summarization with pretrained encoders. August 2019.
- [6] Pranav Rajpurkar, Robin Jia, and Percy Liang. Know what you don’t know: Unanswerable questions for SQuAD. June 2018.
- [7] Chi Sun, Luyao Huang, and Xipeng Qiu. Utilizing BERT for Aspect-Based sentiment analysis via constructing auxiliary sentence. March 2019.
- [8] Mark Chen, Jerry Tworek, Heewoo Jun, Qiming Yuan, Henrique Ponde de Oliveira Pinto, Jared Kaplan, Harri Edwards, Yuri Burda, Nicholas Joseph, Greg Brockman, Alex Ray, Raul Puri, Gretchen Krueger, Michael Petrov, Heidy Khlaaf, Girish Sastry, Pamela Mishkin, Brooke Chan, Scott Gray, Nick Ryder, Mikhail Pavlov, Alethea Power, Lukasz Kaiser, Mohammad Bavarian, Clemens Winter, Philippe Tillet, Felipe Petroski Such, Dave Cummings, Matthias Plappert, Fotios Chantzis, Elizabeth Barnes, Ariel Herbert-Voss, William Hebgen Guss, Alex Nichol, Alex Paino, Nikolas Tezak, Jie Tang, Igor Babuschkin, Suchir Balaji, Shantanu Jain, William Saunders, Christopher Hesse, Andrew N Carr, Jan Leike, Josh Achiam, Vedant Misra, Evan Morikawa, Alec Radford, Matthew Knight, Miles Brundage, Mira Murati, Katie Mayer, Peter Welinder, Bob McGrew, Dario Amodei, Sam McCandlish, Ilya Sutskever, and Wojciech Zaremba. Evaluating large language models trained on code. July 2021.
- [9] Jingxuan He and Martin Vechev. Controlling large language models to generate secure and vulnerable code. February 2023.
- [10] Andrew D White, Glen M Hocky, Heta A Gandhi, Mehrad Ansari, Sam Cox, Geemi P Wellawatte, Subarna Sasmal, Ziyue Yang, Kangxin Liu, Yuvraj Singh, et al. Assessment of chemistry knowledge in large language models that generate code. *Digital Discovery*, 2023.
- [11] Ilias Chalkidis, Ion Androutsopoulos, and Nikolaos Aletras. Neural legal judgment prediction in english. June 2019.
- [12] Tiffany H Kung, Morgan Cheatham, Arielle Medenilla, Czarina Sillos, Lorie De Leon, Camille Elepaño, Maria Madriaga, Rimel Aggabao, Giezel Diaz-Candido, James Maningo, and Victor Tseng. Performance of ChatGPT on USMLE: Potential for AI-assisted medical education using large language models. *PLOS Digit Health*, 2(2): e0000198, February 2023. ISSN 2767-3170. doi:10.1371/journal.pdig.0000198.
- [13] Johan Bollen, Huina Mao, and Xiaojun Zeng. Twitter mood predicts the stock market. *J. Comput. Sci.*, 2(1):1–8, March 2011. ISSN 1877-7503. doi:10.1016/j.jocs.2010.12.007.
- [14] Gunther Eysenbach. The role of ChatGPT, generative language models, and artificial intelligence in medical education: A conversation with ChatGPT and a call for papers. *JMIR Med Educ*, 9:e46885, March 2023. ISSN 2369-3762. doi:10.2196/46885.
- [15] Enkelejda Kasneci, Kathrin Sessler, Stefan Küchemann, Maria Bannert, Daryna Dementieva, Frank Fischer, Urs Gasser, Georg Groh, Stephan Günemann, Eyke Hüllermeier, Stepha Krusche, Gitta Kutyniok, Tilman Michaeli, Claudia Nerdel, Jürgen Pfeffer, Oleksandra Poquet, Michael Sailer, Albrecht Schmidt, Tina Seidel, Matthias Stadler, Jochen Weller, Jochen Kuhn, and Gjergji Kasneci. ChatGPT for good? on opportunities and challenges of large language models for education. *Learn. Individ. Differ.*, 103:102274, April 2023. ISSN 1041-6080. doi:10.1016/j.lindif.2023.102274.
- [16] Emilio Ferrara. What types of COVID-19 conspiracies are populated by twitter bots? April 2020.
- [17] Glen Coppersmith, Mark Dredze, and Craig Harman. Quantifying mental health signals in twitter. In *Proceedings of the Workshop on Computational Linguistics and Clinical Psychology: From Linguistic Signal to Clinical Reality*, Stroudsburg, PA, USA, 2014. Association for Computational Linguistics. doi:10.3115/v1/w14-3207.
- [18] Elizabeth Clark, Yangfeng Ji, and Noah A Smith. Neural text generation in stories using entity representations as context. In *Proceedings of the 2018 Conference of the North American Chapter of the Association for Computational Linguistics: Human Language Technologies, Volume 1 (Long Papers)*, pages 2250–2260, New Orleans, Louisiana, June 2018. Association for Computational Linguistics. doi:10.18653/v1/N18-1204.
- [19] Cheng-Zhi Anna Huang, Ashish Vaswani, Jakob Uszkoreit, Noam Shazeer, Ian Simon, Curtis Hawthorne, Andrew M Dai, Matthew D Hoffman, Monica Dinulescu, and Douglas Eck. Music transformer. September 2018.
- [20] Yunqiu Xu, Ling Chen, Meng Fang, Yang Wang, and Chengqi Zhang. Deep reinforcement learning with transformers for text adventure games. In *2020 IEEE Conference on Games (CoG)*, pages 65–72, August 2020. doi:10.1109/CoG47356.2020.9231622.

- [21] Michiko Yoshitake, Fumitaka Sato, Hiroyuki Kawano, and Hiroshi Teraoka. MaterialBERT for natural language processing of materials science texts. *Science and Technology of Advanced Materials: Methods*, 2(1):372–380, December 2022. doi:10.1080/27660400.2022.2124831.
- [22] Nihang Fu, Lai Wei, Yuqi Song, Qinyang Li, Rui Xin, Sadman Sadeed Omea, Rongzhi Dong, Edirisuriya M Dilanga Siriwardane, and Jianjun Hu. Materials transformers language models for generative materials design: a benchmark study. June 2022.
- [23] Lai Wei, Qinyang Li, Yuqi Song, Stanislav Stefanov, Edirisuriya M D Siriwardane, Fanglin Chen, and Jianjun Hu. Crystal transformer: Self-learning neural language model for generative and tinkering design of materials. April 2022.
- [24] Rongzhi Dong, Yuqi Song, Edirisuriya M D Siriwardane, and Jianjun Hu. Discovery of 2D materials using transformer network based generative design. January 2023.
- [25] Philippe Schwaller, Daniel Probst, Alain C Vaucher, Vishnu H Nair, David Kreutter, Teodoro Laino, and Jean-Louis Reymond. Mapping the space of chemical reactions using attention-based neural networks. *Nature Machine Intelligence*, 3(2):144–152, January 2021. ISSN 2522-5839, 2522-5839. doi:10.1038/s42256-020-00284-w.
- [26] Philippe Schwaller, Alain C Vaucher, Ruben Laplaza, Charlotte Bunne, Andreas Krause, Clemence Corminboeuf, and Teodoro Laino. Machine intelligence for chemical reaction space. *Wiley Interdiscip. Rev. Comput. Mol. Sci.*, 12(5), September 2022. ISSN 1759-0876, 1759-0884. doi:10.1002/wcms.1604.
- [27] Philippe Schwaller, Teodoro Laino, Théophile Gaudin, Peter Bolgar, Christopher A Hunter, Costas Bekas, and Alpha A Lee. Molecular transformer: A model for Uncertainty-Calibrated chemical reaction prediction. *ACS Cent Sci*, 5(9):1572–1583, September 2019. ISSN 2374-7943. doi:10.1021/acscentsci.9b00576.
- [28] Sheng Wang, Yuzhi Guo, Yuhong Wang, Hongmao Sun, and Junzhou Huang. SMILES-BERT: Large scale unsupervised Pre-Training for molecular property prediction. In *Proceedings of the 10th ACM International Conference on Bioinformatics, Computational Biology and Health Informatics, BCB '19*, pages 429–436, New York, NY, USA, September 2019. Association for Computing Machinery. ISBN 9781450366663. doi:10.1145/3307339.3342186.
- [29] Paul G Francoeur and David R Koes. SolTranNet-A machine learning tool for fast aqueous solubility prediction. *J. Chem. Inf. Model.*, 61(6):2530–2536, June 2021. ISSN 1549-9596, 1549-960X. doi:10.1021/acs.jcim.1c00331.
- [30] Jiahui Yu, Chengwei Zhang, Yingying Cheng, Yun-Fang Yang, Yuan-Bin She, Fengfan Liu, WeiKe Su, and An Su. SolvBERT for solvation free energy and solubility prediction: a demonstration of an NLP model for predicting the properties of molecular complexes. *ChemRxiv*, July 2022. doi:10.26434/chemrxiv-2022-0h15p.
- [31] Andrew E Blanchard, John Gounley, Debsindhu Bhowmik, Mayanka Chandra Shekar, Isaac Lyngaas, Shang Gao, Junqi Yin, Aristeidis Tsaris, Feiyi Wang, and Jens Glaser. Language models for the prediction of SARS-CoV-2 inhibitors. *Int. J. High Perform. Comput. Appl.*, 36(5-6):587–602, November 2022. ISSN 1094-3420. doi:10.1177/10943420221121804.
- [32] Changwen Xu, Yuyang Wang, and Amir Barati Farimani. TransPolymer: a transformer-based language model for polymer property predictions. September 2022.
- [33] Jerret Ross, Brian Belgodere, Vijil Chenthamarakshan, Inkit Padhi, Youssef Mroueh, and Payel Das. Molformer: Large scale chemical language representations capture molecular structure and properties. May 2022.
- [34] Kevin Maik Jablonka, Philippe Schwaller, Andres Ortega-Guerrero, and Berend Smit. Is GPT-3 all you need for low-data discovery in chemistry? *ChemRxiv*, February 2023. doi:10.26434/chemrxiv-2023-fw8n4.
- [35] Shion Honda, Shoi Shi, and Hiroki R Ueda. SMILES transformer: Pre-trained molecular fingerprint for low data drug discovery. November 2019.
- [36] Hakime Öztürk, Arzucan Özgür, Philippe Schwaller, Teodoro Laino, and Elif Ozkirimli. Exploring chemical space using natural language processing methodologies for drug discovery. *Drug Discov. Today*, 25(4):689–705, April 2020. ISSN 1359-6446, 1878-5832. doi:10.1016/j.drudis.2020.01.020.
- [37] Zhichao Liu, Ruth A Roberts, Madhu Lal-Nag, Xi Chen, Ruili Huang, and Weida Tong. AI-based language models powering drug discovery and development. *Drug Discov. Today*, 26(11):2593–2607, November 2021. ISSN 1359-6446, 1878-5832. doi:10.1016/j.drudis.2021.06.009.
- [38] Ashish Vaswani, Noam Shazeer, Niki Parmar, Jakob Uszkoreit, Llion Jones, Aidan N Gomez, Lukasz Kaiser, and Illia Polosukhin. Attention is all you need. June 2017.
- [39] Alec Radford, Jeff Wu, Rewon Child, David Luan, Dario Amodei, and Ilya Sutskever. Language models are unsupervised multitask learners. 2019.

- [40] Tom B Brown, Benjamin Mann, Nick Ryder, Melanie Subbiah, Jared Kaplan, Prafulla Dhariwal, Arvind Neelakantan, Pranav Shyam, Girish Sastry, Amanda Askell, Sandhini Agarwal, Ariel Herbert-Voss, Gretchen Krueger, Tom Henighan, Rewon Child, Aditya Ramesh, Daniel M Ziegler, Jeffrey Wu, Clemens Winter, Christopher Hesse, Mark Chen, Eric Sigler, Mateusz Litwin, Scott Gray, Benjamin Chess, Jack Clark, Christopher Berner, Sam McCandlish, Alec Radford, Ilya Sutskever, and Dario Amodei. Language models are Few-Shot learners. May 2020.
- [41] Tuan Dinh, Yuchen Zeng, Ruisu Zhang, Ziqian Lin, Michael Gira, Shashank Rajput, Jy-Yong Sohn, Dimitris Papailiopoulos, and Kangwook Lee. LIFT: Language-Interfaced Fine-Tuning for Non-Language machine learning tasks. June 2022.
- [42] Peter I Frazier. A tutorial on bayesian optimization. July 2018.
- [43] John S Delaney. ESOL: estimating aqueous solubility directly from molecular structure. *J. Chem. Inf. Comput. Sci.*, 44(3):1000–1005, 2004. ISSN 0095-2338. doi:10.1021/ci034243x.
- [44] Thanh Nhat Nguyen, Thuy Tran Phuong Nhat, Ken Takimoto, Ashutosh Thakur, Shun Nishimura, Junya Ohyama, Itsuki Miyazato, Lauren Takahashi, Jun Fujima, Keisuke Takahashi, and Toshiaki Taniike. High-Throughput experimentation and catalyst informatics for oxidative coupling of methane. *ACS Catal.*, 10(2):921–932, January 2020. doi:10.1021/acscatal.9b04293.
- [45] Ryan J Witzke, Alon Chapovetsky, Matthew P Conley, David M Kaphan, and Massimiliano Delferro. Nontraditional catalyst supports in surface organometallic chemistry. *ACS Catal.*, 10(20):11822–11840, October 2020. doi:10.1021/acscatal.0c03350.
- [46] Manuel Moliner, Yuriy Román-Leshkov, and Avelino Corma. Machine learning applied to zeolite synthesis: The missing link for realizing High-Throughput discovery. *Acc. Chem. Res.*, 52(10):2971–2980, October 2019. ISSN 0001-4842, 1520-4898. doi:10.1021/acs.accounts.9b00399.
- [47] Wenhong Yang, Timothy Tizhe Fidelis, and Wen-Hua Sun. Machine learning in catalysis, from proposal to practicing. *ACS Omega*, 5(1):83–88, January 2020. ISSN 2470-1343. doi:10.1021/acsomega.9b03673.
- [48] Jacques A Esterhuizen, Bryan R Goldsmith, and Suljo Linic. Interpretable machine learning for knowledge generation in heterogeneous catalysis. *Nature Catalysis*, 5(3):175–184, March 2022. ISSN 2520-1158, 2520-1158. doi:10.1038/s41929-022-00744-z.
- [49] Felix Musil, Andrea Grisafi, Albert P Bartók, Christoph Ortner, Gábor Csányi, and Michele Ceriotti. Physics-Inspired structural representations for molecules and materials. *Chem. Rev.*, 121(16):9759–9815, August 2021. ISSN 0009-2665, 1520-6890. doi:10.1021/acs.chemrev.1c00021.
- [50] Simon Axelrod, Daniel Schwalbe-Koda, Somesh Mohapatra, James Damewood, Kevin P Greenman, and Rafael Gómez-Bombarelli. Learning matter: Materials design with machine learning and atomistic simulations. *Acc. Mater. Res.*, 3(3):343–357, March 2022. doi:10.1021/accountsmr.1c00238.
- [51] Vahe Tshitoyan, John Dagdelen, Leigh Weston, Alexander Dunn, Ziqin Rong, Olga Kononova, Kristin A Persson, Gerbrand Ceder, and Anubhav Jain. Unsupervised word embeddings capture latent knowledge from materials science literature. *Nature*, 571(7763):95–98, 2019.
- [52] Hasan M Sayeed, Sterling G Baird, and Taylor D Sparks. Structure feature vectors derived from robcystallographer text descriptions of crystal structures using word embeddings. 2023.
- [53] Murat Cihan Sorkun, Abhishek Khetan, and Süleyman Er. AqSolDB, a curated reference set of aqueous solubility and 2D descriptors for a diverse set of compounds. *Sci Data*, 6(1):143, August 2019. ISSN 2052-4463. doi:10.1038/s41597-019-0151-1.
- [54] Andrew P Abbott, Glen Capper, David L Davies, Raymond K Rasheed, and Vasuki Tambyrajah. Novel solvent properties of choline chloride/urea mixtures. *Chem. Commun.*, (1):70–71, January 2003. ISSN 1359-7345. doi:10.1039/b210714g.
- [55] Ulf Norinder and Christel A S Bergström. Prediction of ADMET properties. *ChemMedChem*, 1(9):920–937, September 2006. ISSN 1860-7179. doi:10.1002/cmdc.200600155.
- [56] Robert Docherty, Klimentina Pencheva, and Yuriy A Abramov. Low solubility in drug development: deconvoluting the relative importance of solvation and crystal packing. *J. Pharm. Pharmacol.*, 67(6):847–856, June 2015. ISSN 0022-3573, 2042-7158. doi:10.1111/jphp.12393.
- [57] Jaclyn A Barrett, Wenzhan Yang, Suzanne M Skolnik, Lisa M Belliveau, and Kellyn M Patros. Discovery solubility measurement and assessment of small molecules with drug development in mind. *Drug Discov. Today*, 27(5):1315–1325, May 2022. ISSN 1359-6446, 1878-5832. doi:10.1016/j.drudis.2022.01.017.

- [58] Pietro Sormanni, Francesco A Aprile, and Michele Vendruscolo. The CamSol method of rational design of protein mutants with enhanced solubility. *J. Mol. Biol.*, 427(2):478–490, January 2015. ISSN 0022-2836, 1089-8638. doi:10.1016/j.jmb.2014.09.026.
- [59] Antonio Llinàs, Robert C Glen, and Jonathan M Goodman. Solubility challenge: can you predict solubilities of 32 molecules using a database of 100 reliable measurements? *J. Chem. Inf. Model.*, 48(7):1289–1303, July 2008. ISSN 1549-9596. doi:10.1021/ci800058v.
- [60] Antonio Llinas and Alex Avdeef. Solubility challenge revisited after ten years, with multilab Shake-Flask data, using tight (SD 0.17 log) and loose (SD 0.62 log) test sets. *J. Chem. Inf. Model.*, 59(6):3036–3040, June 2019. ISSN 1549-9596, 1549-960X. doi:10.1021/acs.jcim.9b00345.
- [61] David S Palmer and John B O Mitchell. Is experimental data quality the limiting factor in predicting the aqueous solubility of druglike molecules? *Mol. Pharm.*, 11(8):2962–2972, August 2014. ISSN 1543-8384, 1543-8392. doi:10.1021/mp500103r.
- [62] R E Skyner, J L McDonagh, C R Groom, T van Mourik, and J B O Mitchell. A review of methods for the calculation of solution free energies and the modelling of systems in solution. *Phys. Chem. Chem. Phys.*, 17(9): 6174–6191, March 2015. ISSN 1463-9076, 1463-9084. doi:10.1039/c5cp00288e.
- [63] James L McDonagh, Neetika Nath, Luna De Ferrari, Tanja van Mourik, and John B O Mitchell. Uniting cheminformatics and chemical theory to predict the intrinsic aqueous solubility of crystalline druglike molecules. *J. Chem. Inf. Model.*, 54(3):844–856, March 2014. ISSN 1549-9596, 1549-960X. doi:10.1021/ci4005805.
- [64] Wenlu Wang, Ye Wang, Honggang Zhao, and Simone Sciabola. A transformer-based generative model for DE novo molecular design. October 2022. doi:10.48550/ARXIV.2210.08749.
- [65] Łukasz Maziarka, Tomasz Danel, Sławomir Mucha, Krzysztof Rataj, Jacek Tabor, and Stanisław Jastrzębski. Molecule attention transformer. *arXiv preprint arXiv:2002.08264*, 2020.
- [66] Ziyue Yang, Katarina A Milas, and Andrew D White. Now what sequence? pre-trained ensembles for bayesian optimization of protein sequences. *bioRxiv*, pages 2022–08, 2022.
- [67] Nathan Frey, Ryan Soklaski, Simon Axelrod, Siddharth Samsi, Rafael Gomez-Bombarelli, Connor Coley, and Vijay Gadepally. Neural scaling of deep chemical models. 2022.
- [68] Gayane Chilingaryan, Hovhannes Tamoyan, Ani Tevosyan, Nelly Babayan, Lusine Khondkaryan, Karen Hambardzumyan, Zaven Navoyan, Hrant Khachatryan, and Armen Aghajanyan. Bartsmliles: Generative masked language models for molecular representations. *arXiv preprint arXiv:2211.16349*, 2022.
- [69] Ross Irwin, Spyridon Dimitriadis, Jiazhen He, and Esben Jannik Bjerrum. Chemformer: a pre-trained transformer for computational chemistry. *Machine Learning: Science and Technology*, 3(1):015022, 2022.
- [70] Philippe Schwaller, Alain C Vaucher, Teodoro Laino, and Jean-Louis Reymond. Prediction of chemical reaction yields using deep learning. *Machine learning: science and technology*, 2(1):015016, 2021.
- [71] Jason Wei, Xuezhi Wang, Dale Schuurmans, Maarten Bosma, Ed Chi, Quoc Le, and Denny Zhou. Chain of thought prompting elicits reasoning in large language models. *arXiv preprint arXiv:2201.11903*, 2022.
- [72] Takeshi Kojima, Shixiang Shane Gu, Machel Reid, Yutaka Matsuo, and Yusuke Iwasawa. Large language models are zero-shot reasoners. *arXiv preprint arXiv:2205.11916*, 2022.
- [73] Jaehun Jung, Lianhui Qin, Sean Welleck, Faeze Brahman, Chandra Bhagavatula, Ronan Le Bras, and Yejin Choi. Maieutic prompting: Logically consistent reasoning with recursive explanations. *arXiv preprint arXiv:2205.11822*, 2022.
- [74] Hattie Zhou, Azade Nova, Hugo Larochelle, Aaron Courville, Behnam Neyshabur, and Hanie Sedghi. Teaching algorithmic reasoning via in-context learning. *arXiv preprint arXiv:2211.09066*, 2022.
- [75] Qing Lyu, Shreya Havaldar, Adam Stein, Li Zhang, Delip Rao, Eric Wong, Marianna Apidianaki, and Chris Callison-Burch. Faithful chain-of-thought reasoning. *arXiv preprint arXiv:2301.13379*, 2023.
- [76] Denny Zhou, Nathanael Schärli, Le Hou, Jason Wei, Nathan Scales, Xuezhi Wang, Dale Schuurmans, Olivier Bousquet, Quoc Le, and Ed Chi. Least-to-most prompting enables complex reasoning in large language models. *arXiv preprint arXiv:2205.10625*, 2022.
- [77] Damai Dai, Yutao Sun, Li Dong, Yaru Hao, Zhifang Sui, and Furu Wei. Why can gpt learn in-context? language models secretly perform gradient descent as meta optimizers. *arXiv preprint arXiv:2212.10559*, 2022.
- [78] Bobak Shahriari, Kevin Swersky, Ziyu Wang, Ryan P Adams, and Nando de Freitas. Taking the human out of the loop: A review of bayesian optimization. *Proceedings of the IEEE*, 104(1):148–175, 2015.

- [79] Qiaohao Liang, Aldair E Gongora, Zekun Ren, Armi Tiihonen, Zhe Liu, Shijing Sun, James R Deneault, Daniil Bash, Flore Mekki-Berrada, Saif A Khan, Kedar Hippalgaonkar, Benji Maruyama, Keith A Brown, John Fisher, III, and Tonio Buonassisi. Benchmarking the performance of bayesian optimization across multiple experimental materials science domains. *npj Computational Materials*, 7(1):1–10, November 2021. ISSN 2057-3960, 2057-3960. doi:10.1038/s41524-021-00656-9.
- [80] Sterling G. Baird, Marianne Liu, and Taylor D. Sparks. High-dimensional bayesian optimization of 23 hyperparameters over 100 iterations for an attention-based network to predict materials property: A case study on CrabNet using ax platform and SAASBO. *Computational Materials Science*, 211:111505, August 2022. doi:10.1016/j.commatsci.2022.111505. URL <https://doi.org/10.1016/j.commatsci.2022.111505>.
- [81] Mani Valletti, Rama K. Vasudevan, Maxim A. Ziatdinov, and Sergei V. Kalinin. Bayesian optimization in continuous spaces via virtual process embeddings. *Digital Discovery*, 1(6):910–925, 2022. doi:10.1039/d2dd00065b. URL <https://doi.org/10.1039/d2dd00065b>.
- [82] Edward O Pyzer-Knapp, Jed W Pitera, Peter W J Staar, Seiji Takeda, Teodoro Laino, Daniel P Sanders, James Sexton, John R Smith, and Alessandro Curioni. Accelerating materials discovery using artificial intelligence, high performance computing and robotics. *npj Computational Materials*, 8(1):84, 2022.
- [83] Turab Lookman, Prasanna V Balachandran, Dezhen Xue, John Hogden, and James Theiler. Statistical inference and adaptive design for materials discovery. *Curr. Opin. Solid State Mater. Sci.*, 21(3):121–128, June 2017. ISSN 1359-0286. doi:10.1016/j.cossms.2016.10.002.
- [84] Jose Miguel Hernandez-Lobato, Daniel Reagen, Ryan P Adams, David Duvenaud, Zoubin Ghahramani, Matt J Kusner, Andreas Scherer, Edward Snelson, Jasper Snoek, Steven Swift, et al. Predictive materials design with high-throughput screening and online optimization. *Machine Learning for Materials Discovery workshop at NIPS*, 2017.
- [85] Natalie S Eyke, William H Green, and Klavs F Jensen. Iterative experimental design based on active machine learning reduces the experimental burden associated with reaction screening. *Reaction Chemistry & Engineering*, 5(10):1963–1972, 2020.
- [86] Harrison Chase. LangChain, 10 2022. URL <https://github.com/hwchase17/langchain>.
- [87] OpenAI. GPT-4 technical report. March 2023.
- [88] Gabriel Murray, Steve Renals, and Jean Carletta. Extractive summarization of meeting recordings. 2005.
- [89] Shengbo Guo and Scott Sanner. Probabilistic latent maximal marginal relevance. In *Proceedings of the 33rd international ACM SIGIR conference on Research and development in information retrieval, SIGIR '10*, pages 833–834, New York, NY, USA, July 2010. Association for Computing Machinery. ISBN 9781450301534. doi:10.1145/1835449.1835639.
- [90] Arvind Neelakantan, Tao Xu, Raul Puri, Alec Radford, Jesse Michael Han, Jerry Tworek, Qiming Yuan, Nikolaus Tezak, Jong Wook Kim, Chris Hallacy, et al. Text and code embeddings by contrastive pre-training. *arXiv preprint arXiv:2201.10005*, 2022.
- [91] Jeff Johnson, Matthijs Douze, and Hervé Jégou. Billion-scale similarity search with gpus. *IEEE Transactions on Big Data*, 7(3):535–547, 2019.
- [92] Michael Ahn, Anthony Brohan, Noah Brown, Yevgen Chebotar, Omar Cortes, Byron David, Chelsea Finn, Keerthana Gopalakrishnan, Karol Hausman, Alex Herzog, et al. Do as i can, not as i say: Grounding language in robotic affordances. *arXiv preprint arXiv:2204.01691*, 2022.
- [93] C. Saunders, A. Gammernan, and V. Vovk. Ridge regression learning algorithm in dual variables. *ICML*, 1998.
- [94] Carl Edward Rasmussen and Christopher K I Williams. *Gaussian Processes for Machine Learning*. MIT Press, November 2005. ISBN 9780262182539.
- [95] Naomi S Altman. An introduction to kernel and nearest-neighbor nonparametric regression. *The American Statistician*, 46(3):175–185, 1992.
- [96] Mukund Balasubramanian and Eric L Schwartz. The isomap algorithm and topological stability. *Science*, 295(5552):7–7, 2002.
- [97] Riley J Hickman, Matteo Aldeghi, Florian Häse, and Alán Aspuru-Guzik. Bayesian optimization with known experimental and design constraints for chemistry applications. *Digital Discovery*, 1(5):732–744, October 2022. ISSN 2635-098X. doi:10.1039/D2DD00028H.
- [98] Luyu Gao, Xueguang Ma, Jimmy Lin, and Jamie Callan. Precise zero-shot dense retrieval without relevance labels. *arXiv preprint arXiv:2212.10496*, 2022.

- [99] Aarohi Srivastava, Abhinav Rastogi, Abhishek Rao, Abu Awal Md Shoeb, Abubakar Abid, Adam Fisch, Adam R Brown, Adam Santoro, Aditya Gupta, Adrià Garriga-Alonso, et al. Beyond the imitation game: Quantifying and extrapolating the capabilities of language models. *arXiv preprint arXiv:2206.04615*, 2022.
- [100] Balaji Lakshminarayanan, Alexander Pritzel, and Charles Blundell. Simple and scalable predictive uncertainty estimation using deep ensembles. December 2016.
- [101] Volodymyr Kuleshov, Nathan Fenner, and Stefano Ermon. Accurate uncertainties for deep learning using calibrated regression. In Jennifer Dy and Andreas Krause, editors, *Proceedings of the 35th International Conference on Machine Learning*, volume 80 of *Proceedings of Machine Learning Research*, pages 2796–2804. PMLR, 2018.
- [102] Youngseog Chung, Ian Char, Han Guo, Jeff Schneider, and Willie Neiswanger. Uncertainty toolbox: an Open-Source library for assessing, visualizing, and improving uncertainty quantification. September 2021.
- [103] Mitchell Juneau, Daphna Yaffe, Renjie Liu, Jane N. Agwara, and Marc D. Porosoff. Establishing tungsten carbides as active catalysts for CO₂ hydrogenation. *Nanoscale*, 14(44):16458–16466, 2022. doi:10.1039/d2nr03281c. URL <https://doi.org/10.1039/d2nr03281c>.
- [104] Benedek Fabian, Thomas Edlich, H el ena Gaspar, Marwin Segler, Joshua Meyers, Marco Fiscato, and Mohamed Ahmed. Molecular representation learning with language models and domain-relevant auxiliary tasks. November 2020.
- [105] Jannis Born and Matteo Manica. Regression transformer: Concurrent sequence regression and generation for molecular language modeling. February 2022.

A Supp. Material

A.1 Solubility

model	prompt	RMSE ↓	MAE ↓	r ↑	neg-ll ↓
text-curie-001	multi	1.791	1.245	0.613	2.218
text-curie-001	topk	1.811	1.245	0.613	2.218
text-davinci-003	topk	1.185	0.814	0.805	1.901
gpt-4	topk	0.773	0.578	0.921	2.564
Fine-tuned (text-ada-001)	topk	1.558	0.852	0.779	4.166
GPR with ada embeddings	topk	2.652	1.129	0.620	1.795
KNN	-	2.443	1.739	0.456	-
SolTranNet[29]	-	2.99			
SMILES-BERT[28]	-	0.47			
MolBERT[104]	-	0.531			
Regression Transformer[105]	-	0.73			
MolFormer[33]	-	0.278			
ESOL[43]	-		0.83	0.74	

Table A.1: Comparison of our ICL models against state-of-the-art(SOTA) models for the solubility dataset. All SOTA models are a kind of transformers model trained from scratch to reproduce solubility on ESOL dataset. Missing data in the table means that the authors did not report the metric in their study. The best value for each metric is displayed in bold. Displayed ICL models represent instances for each model type using the hyperparameters selected by the investigation in which we systematically varied each hyperparameter. For all LLMs, we defined temperature $T = 0.7$, context size $k = 5$, and $N = 700$ training points. All baselines were trained also considering $N = 700$ training points. Displayed metrics were calculated after recalibration.

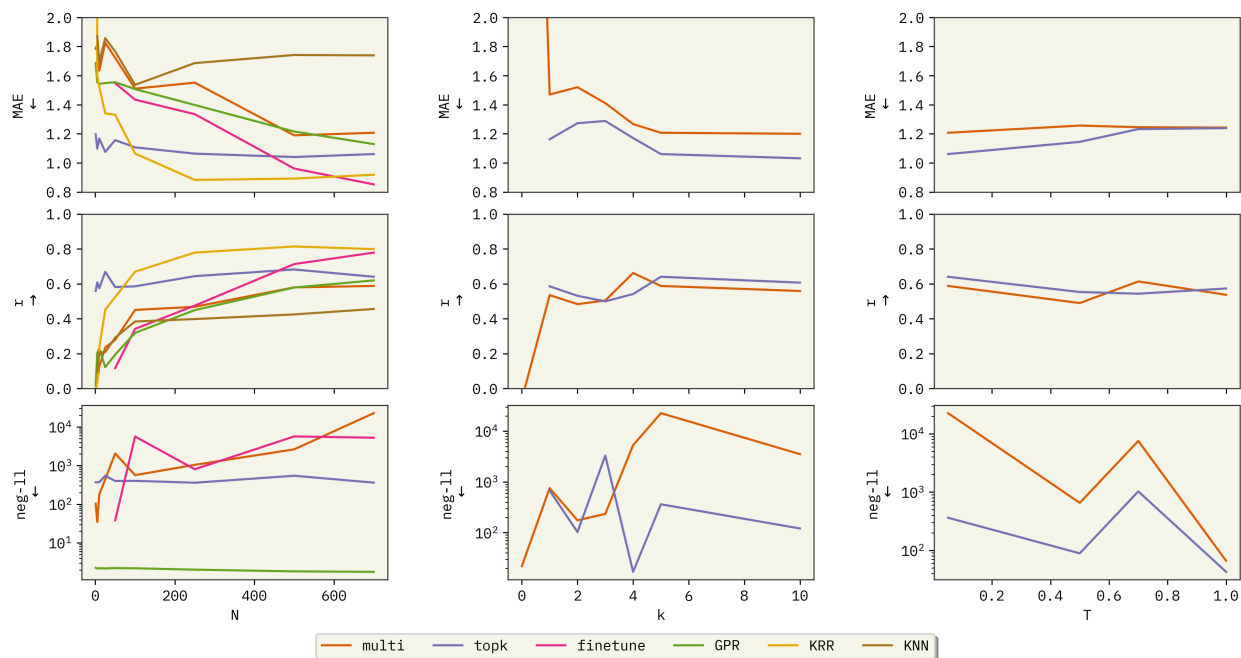


Figure A.1: Metrics with respect to N , k , and T using the `text-curie-001` model on the solubility dataset. The left panel displays The number of training points N , varying from 1 to 700, while keeping the number of examples $k = 5$ and temperature $T = 0.05$ constant. The middle panel illustrates the relationship between the number of examples k used in the context and model performance, with k ranging from 0 to 10, and fixed values of $N = 700$ and $T = 0.05$. The right panel demonstrates the effect of varying the temperature T between 0 and 1, while maintaining $N = 700$ and $k = 5$ constant.

A.1.1 Multi-options prompt

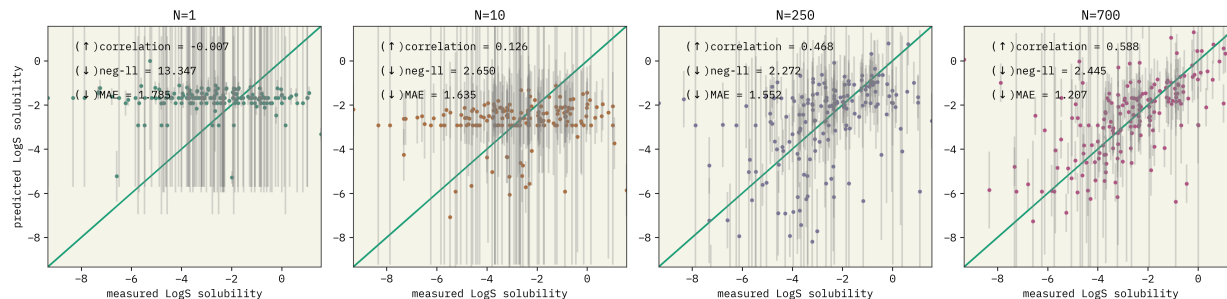


Figure A.2: Calibrated parity plots using `text-curie-001` with Multi-options prompt on the solubility dataset. Those experiments were made by defining the number of examples used as $k = 5$ and temperature $T = 0.05$. The number of training points N from which the model can select the examples was varied in a range from 1 to 700

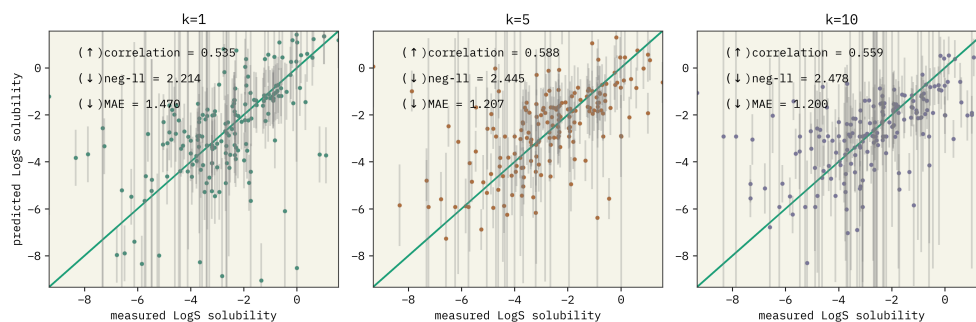


Figure A.3: Calibrated parity plots using `text-curie-001` with Multi-options prompt on the solubility dataset. Those experiments were made by defining the size of the training set as $N = 700$ and temperature $T = 0.05$. The number of selected examples k to create the context was studied. We varied it in a range from 0 to 10. For $k=0$ (zero-shot), the model generated the same values out of the range independent of the request. Therefore, data for $k=0$ is not shown.

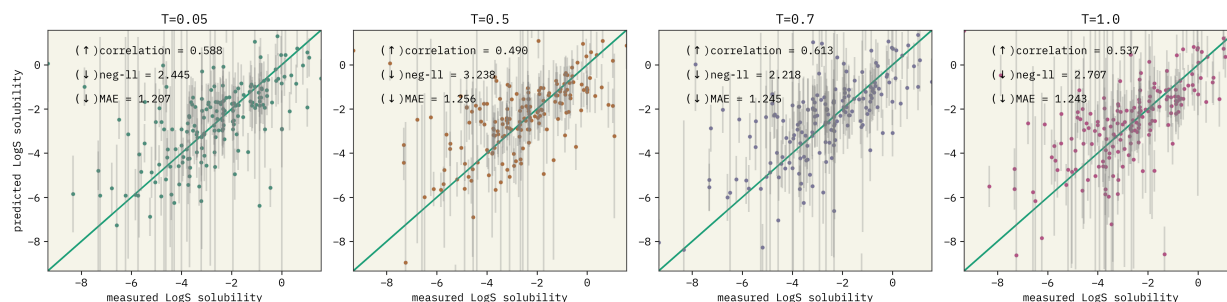


Figure A.4: Calibrated parity plots using `text-curie-001` with Multi-options prompt on the solubility dataset. Those experiments were made by defining the size of the training set as $N = 700$ and context size $k = 5$. The temperature T was varied in a range from 0 to 10.

A.1.2 Top k completions prompt

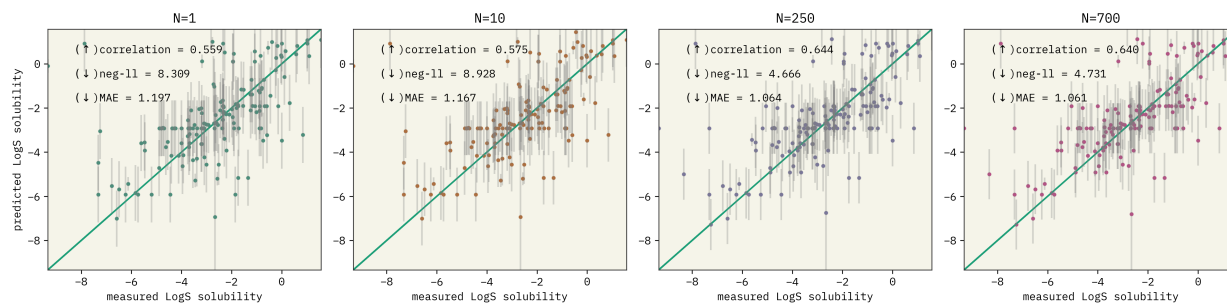


Figure A.5: Calibrated parity plots using `text-curie-001` with `topk completions` prompt on the solubility dataset. Those experiments were made by defining the number of examples used as $k = 5$ and temperature $T = 0.05$. The number of training points N from which the model can select the examples was varied in a range from 1 to 700

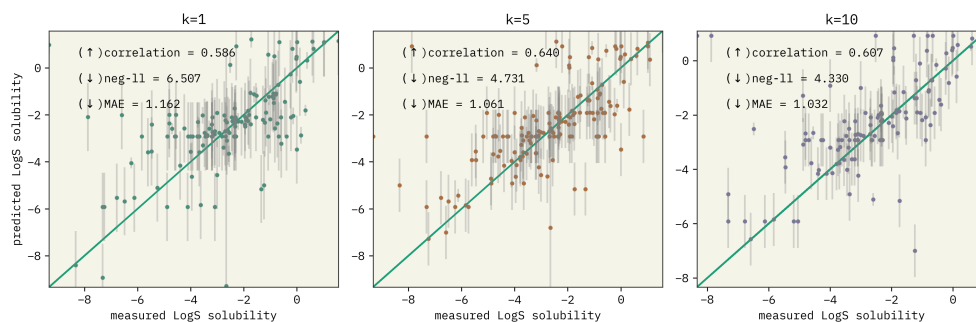


Figure A.6: Calibrated parity plots using `text-curie-001` with `topk completions` prompt on the solubility dataset. Those experiments were made by defining the number of examples used as $N = 700$ and temperature $T = 0.05$. The number of selected examples k to create the context varied in a range from 0 to 10. For $k = 0$ (zero-shot), the model mostly hallucinated and generated non-numeric tokens. Therefore, data for $k=0$ is not shown.

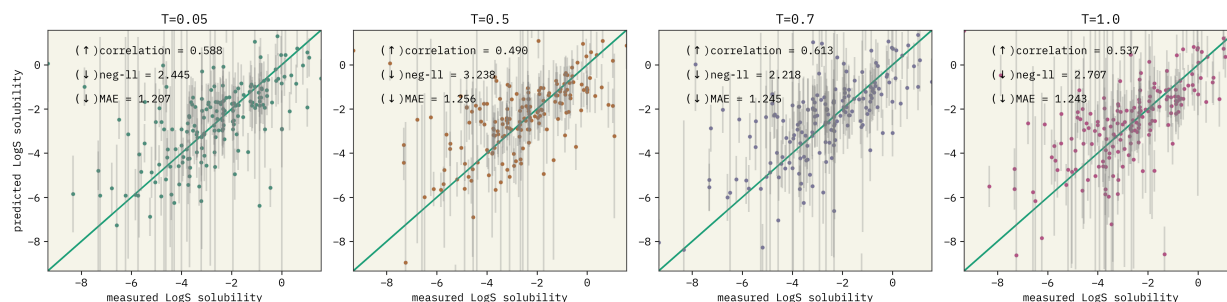


Figure A.7: Calibrated parity plots using `text-curie-001` with `topk completions` prompt on the solubility dataset. Those experiments were made by defining the size of the training set as $N = 700$ and context size $k = 5$. The temperature T was varied in a range from 0 to 1.0.

A.1.3 Finetuning

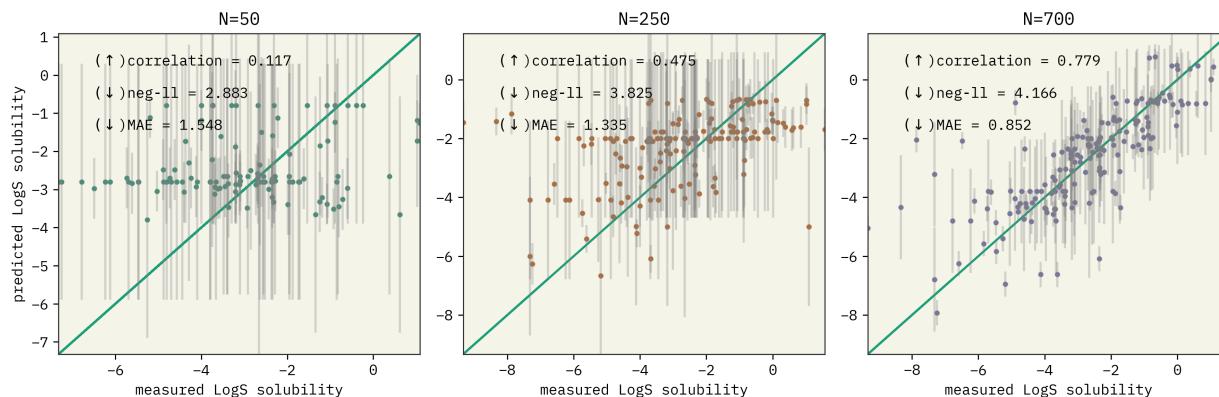


Figure A.8: Calibrated parity plots using fine-tuned `text-ada-001` with `topk completions` prompt on the solubility dataset. Those experiments were made by defining the number of examples used as $k = 0$ and temperature $T = 0.05$. The number of training points N from which the model can select the examples was varied in a range from 50 to 700

A.1.4 GPR

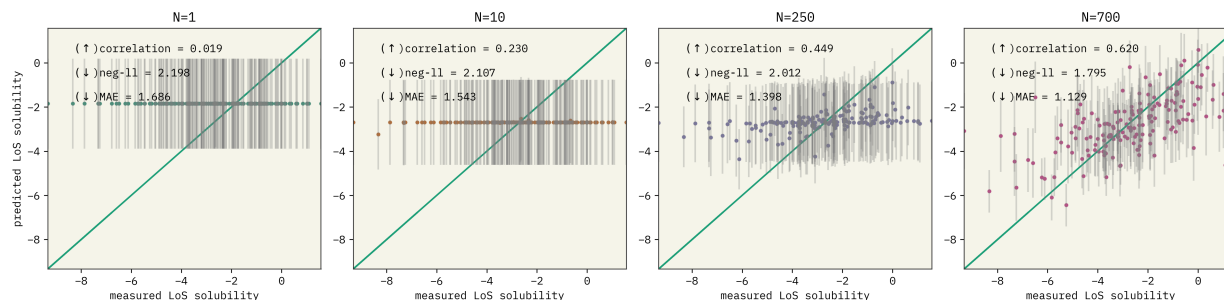


Figure A.9: Metrics with respect to N using Gaussian process regressor(GPR) with `topk completions` prompt on the solubility dataset. To generate the inputs for the GPR, we used `text-embedding-ada-002` to embed the prompt. Those experiments were made by defining the number of examples used as $k = 0$ and temperature $T = 0.05$. The number of training points N from which the model can select the examples was varied in a range from 1 to 700

A.1.5 KNN

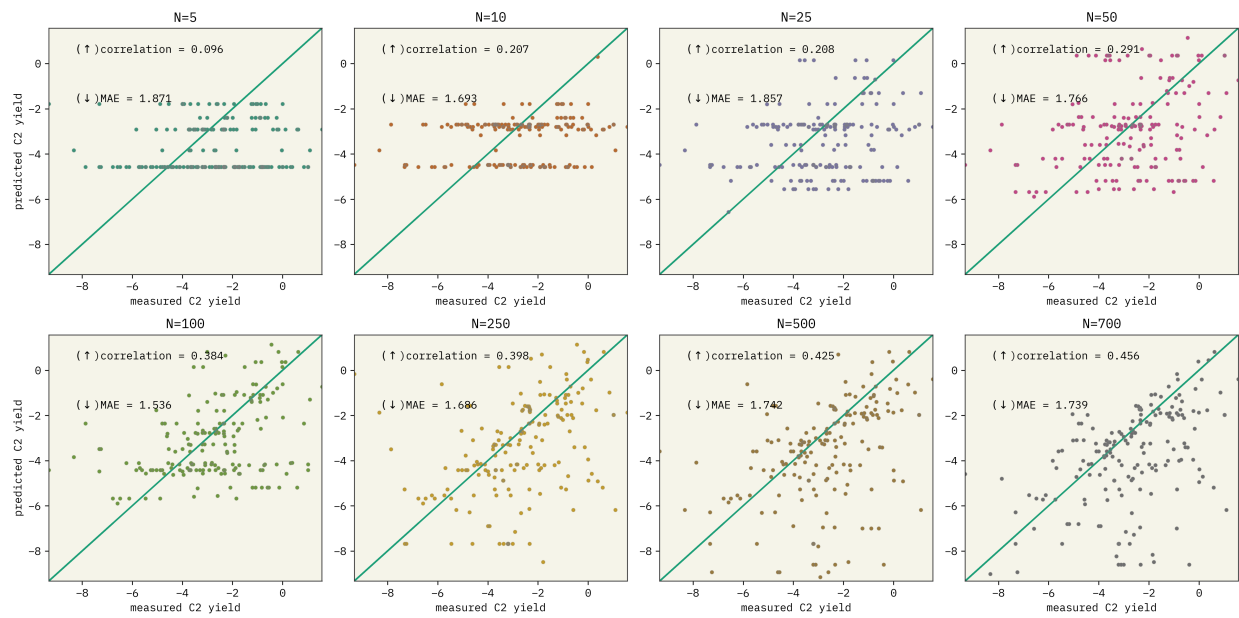


Figure A.10: Metrics with respect to N using Nearest Neighbors(KNN) with topk completions prompt on the solubility dataset. To generate the vectors to select the nearest neighbor, we used `text-embedding-ada-002` to embed the prompt. Those experiments were made by defining the number of examples used as $k = 0$ and temperature $T = 0.05$. The number of training points N from which the model can select the examples was varied in a range from 1 to 700

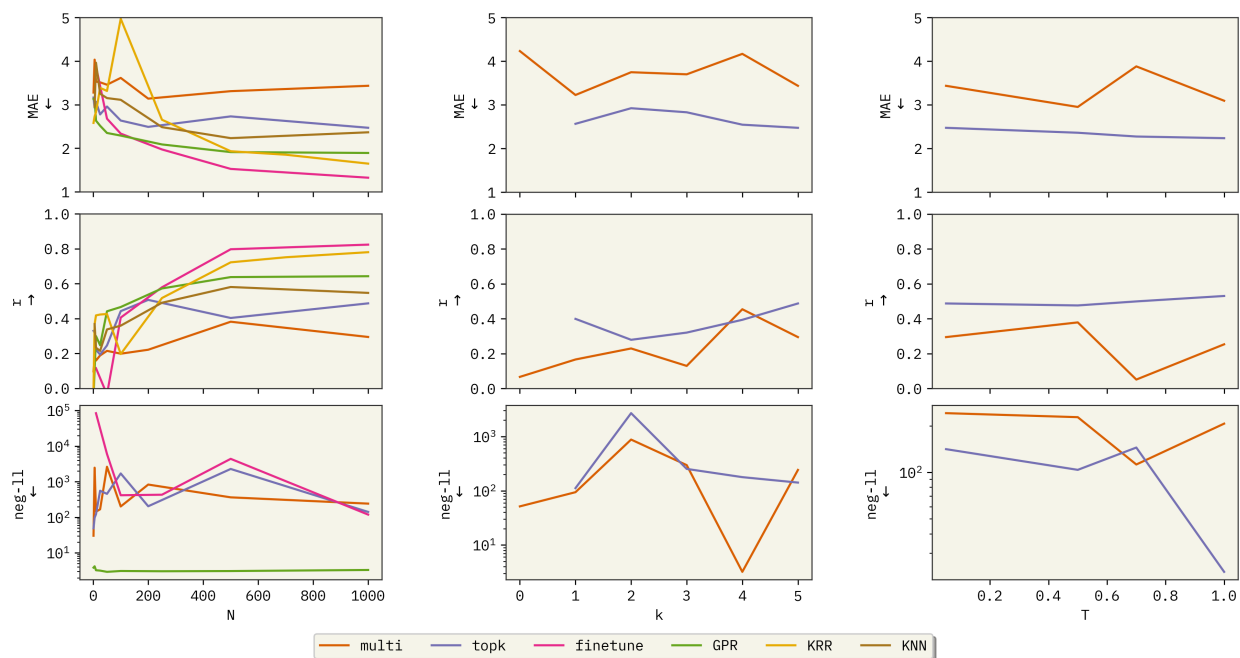
A.2 C₂ yield

Figure A.11: Metrics with respect to N , k , and T using the `text-curie-001` model on the C₂ yield dataset. The left panel displays the number of training points N , varying from 1 to 1000, while keeping the number of examples $k = 5$ and temperature $T = 0.05$ constant. The middle panel illustrates the relationship between the number of examples k used in the context and model performance, with k ranging from 0 to 5, and fixed values of $N = 1000$ and $T = 0.05$. The right panel demonstrates the effect of varying the temperature T between 0 and 1, while maintaining $N = 1000$ and $k = 5$ constant.

A.2.1 Multi-option prompt

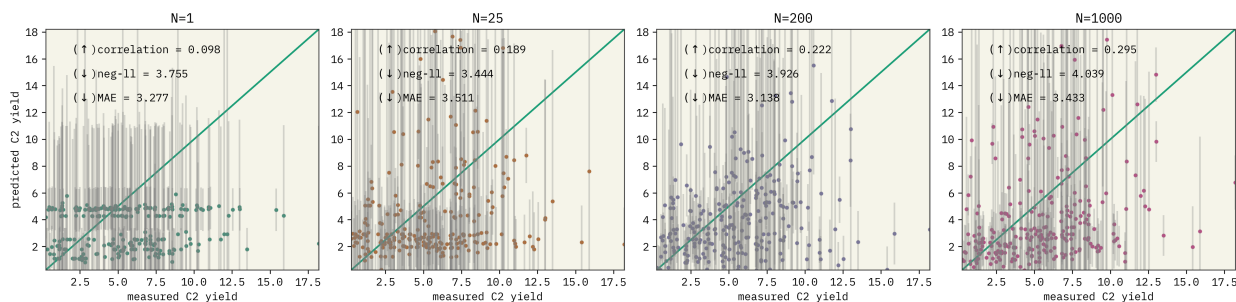


Figure A.12: Calibrated parity plots using `text-curie-001` with Multi-options prompt on the C_2 catalyst dataset. Those experiments were made by defining the number of examples used as $k = 5$ and temperature $T = 0.05$. The number of training points N from which the model can select the examples was varied in a range from 1 to 1000

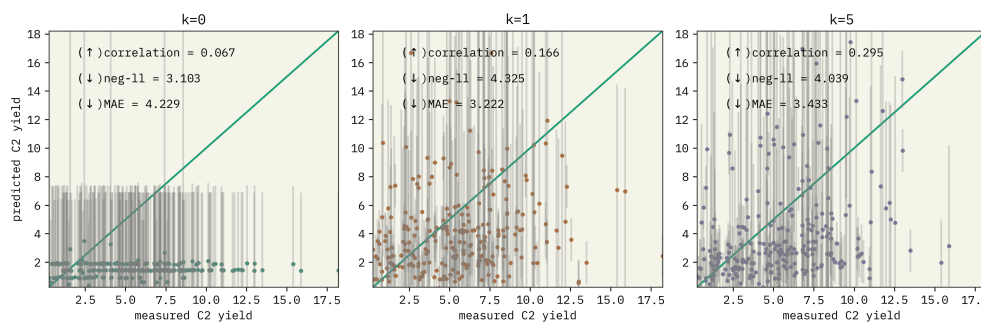


Figure A.13: Calibrated parity plots using `text-curie-001` with Multi-options prompt on the C_2 catalyst dataset. Those experiments were made by defining the number of examples used as $N = 700$ and temperature $T = 0.05$. The number of selected examples k to create the context was varied in a range from 1 to 10.

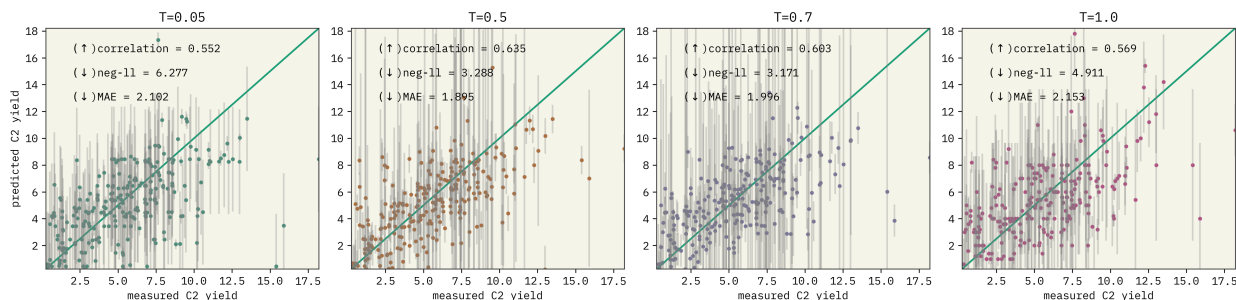


Figure A.14: Calibrated parity plots using `text-curie-001` with Multi-options prompt on the C_2 catalyst dataset. Those experiments were made by defining the number of examples used as $N = 700$ and the number of examples $k = 5$. The temperature T to generate the completions was varied in a range from 0.05 to 1.0.

A.2.2 Top k completions prompt

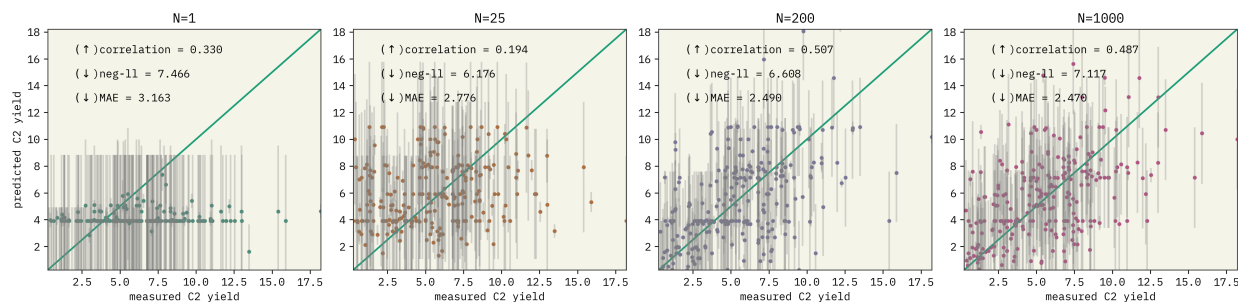


Figure A.15: Calibrated parity plots using `text-curie-001` with Topk completions prompt on the C_2 catalyst dataset. Those experiments were made by defining the number of examples used as $k = 5$ and temperature $T = 0.05$. The number of training points N from which the model can select the examples was varied in a range from 1 to 1000

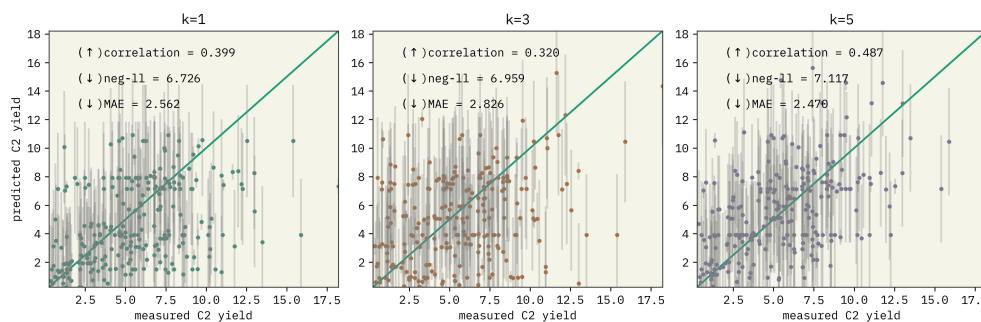


Figure A.16: Calibrated parity plots using `text-curie-001` with Topk completions prompt on the C_2 catalyst dataset. Those experiments were made by defining the number of examples used as $N = 700$ and temperature $T = 0.05$. The number of selected examples k to create the context was varied in a range from 1 to 10.

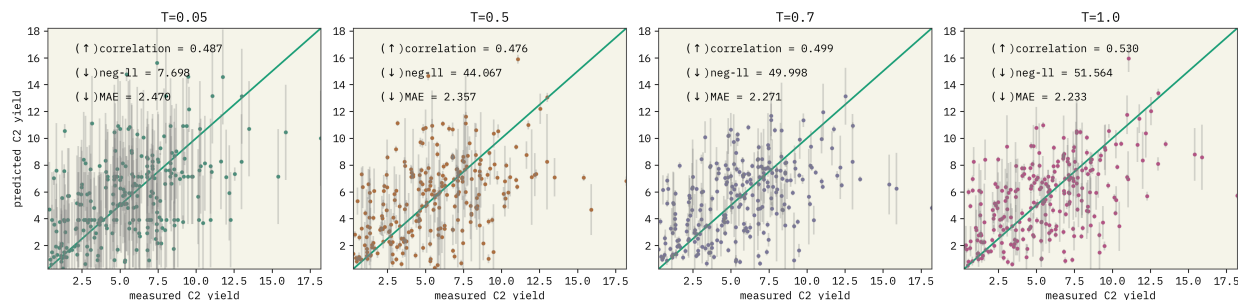


Figure A.17: Calibrated parity plots using `text-curie-001` with Topk completions prompt on the C_2 catalyst dataset. Those experiments were made by defining the number of examples used as $N = 700$ and the number of examples $k = 5$. The temperature T to generate the completions was varied in a range from 0.05 to 1.0.

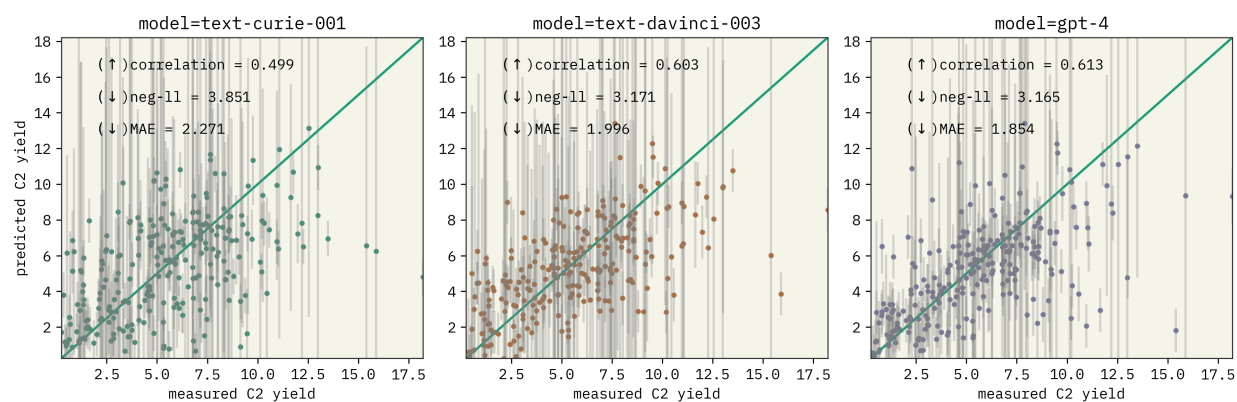


Figure A.18: Calibrated parity plots using different models with Multi-options prompt on the C₂ catalyst dataset. We considered `text-curie-001`, `text-davinci-003`, and `gpt-4` defining the number of examples used as $N = 1000$, the number of examples $k = 5$ and temperature $T = 0.7$.

A.2.3 Finetuning

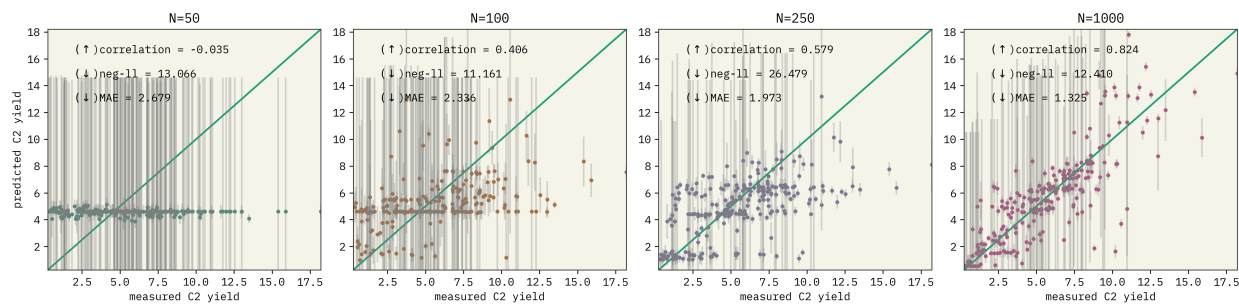


Figure A.19: Calibrated parity plots using fine-tuned `text-ada-001` with `topk completions` prompt on the C_2 catalyst dataset. Those experiments were made by defining the number of examples used as $k = 0$ and temperature $T = 0.05$. The number of training points N from which the model can select the examples was varied in a range from 50 to 1000

A.2.4 GPR

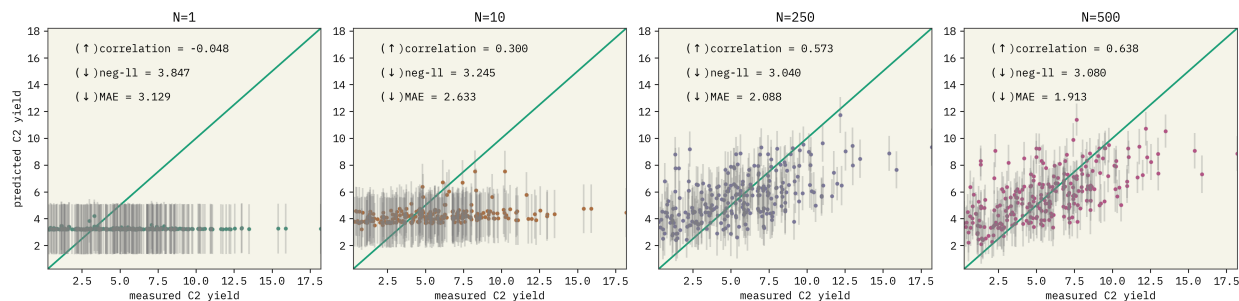


Figure A.20: Metrics with respect to N using Gaussian process regressor (GPR) with `topk completions` prompt on the C_2 catalyst dataset. To generate the inputs for the GPR, we used `text-embedding-ada-002` to embed the prompt. Those experiments were made by defining the number of examples used as $k = 0$ and temperature $T = 0.05$. The number of training points N from which the model can select the examples was varied in a range from 1 to 500

A.2.5 GPR

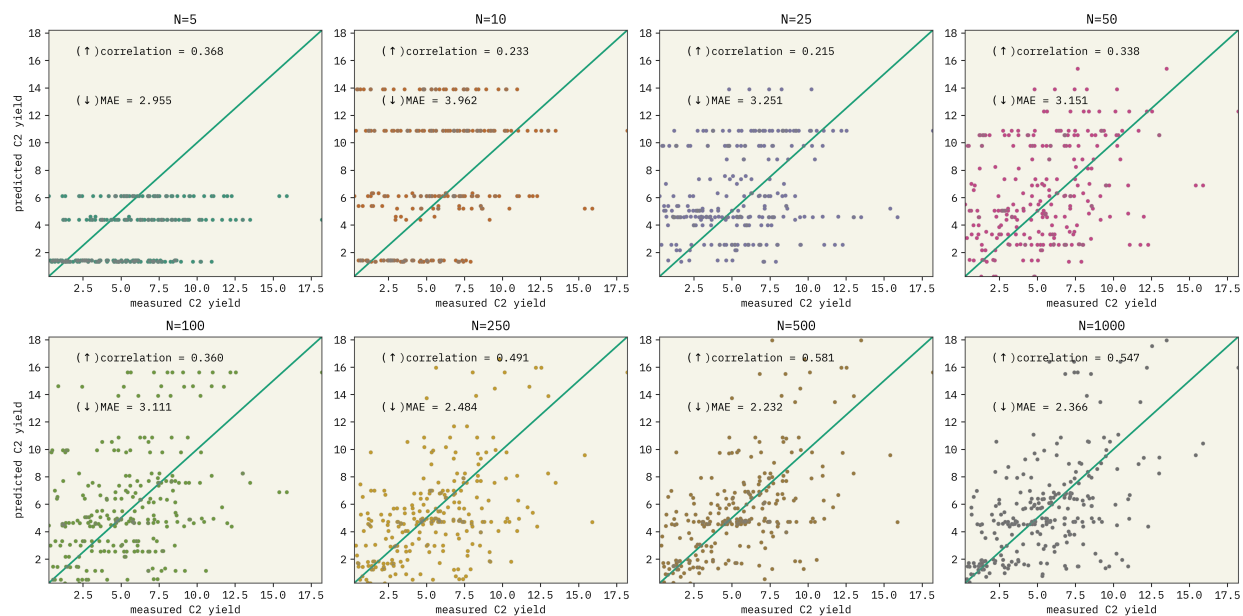


Figure A.21: Metrics with respect to N using NearestNeighbor (KNN) with topk completions prompt on the C₂ catalyst dataset. To generate embedding to select the nearest neighbors, we used `text-embedding-ada-002` to embed the prompt. Those experiments were made by defining the number of examples used as $k = 0$ and temperature $T = 0.05$. The number of training points N from which the model can select the examples was varied in a range from 1 to 500

A.3 Calibration

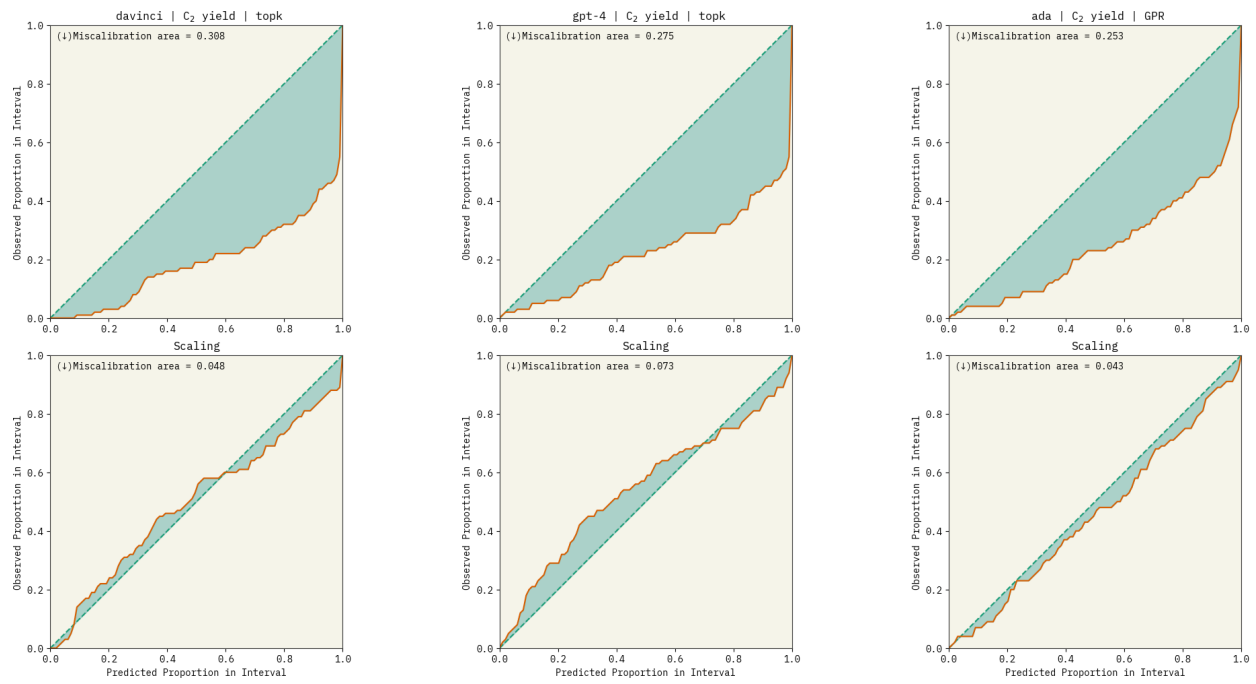


Figure A.22: Miscalibration analysis and correction using Uncertainty-toolbox to introduce a corrective scaling-factor used for regression tasks: davinci | topk (3.783), gpt-4 | topk (4.330), ada | gpr (2.110)

B Inverse design

B.1 Reaction Results

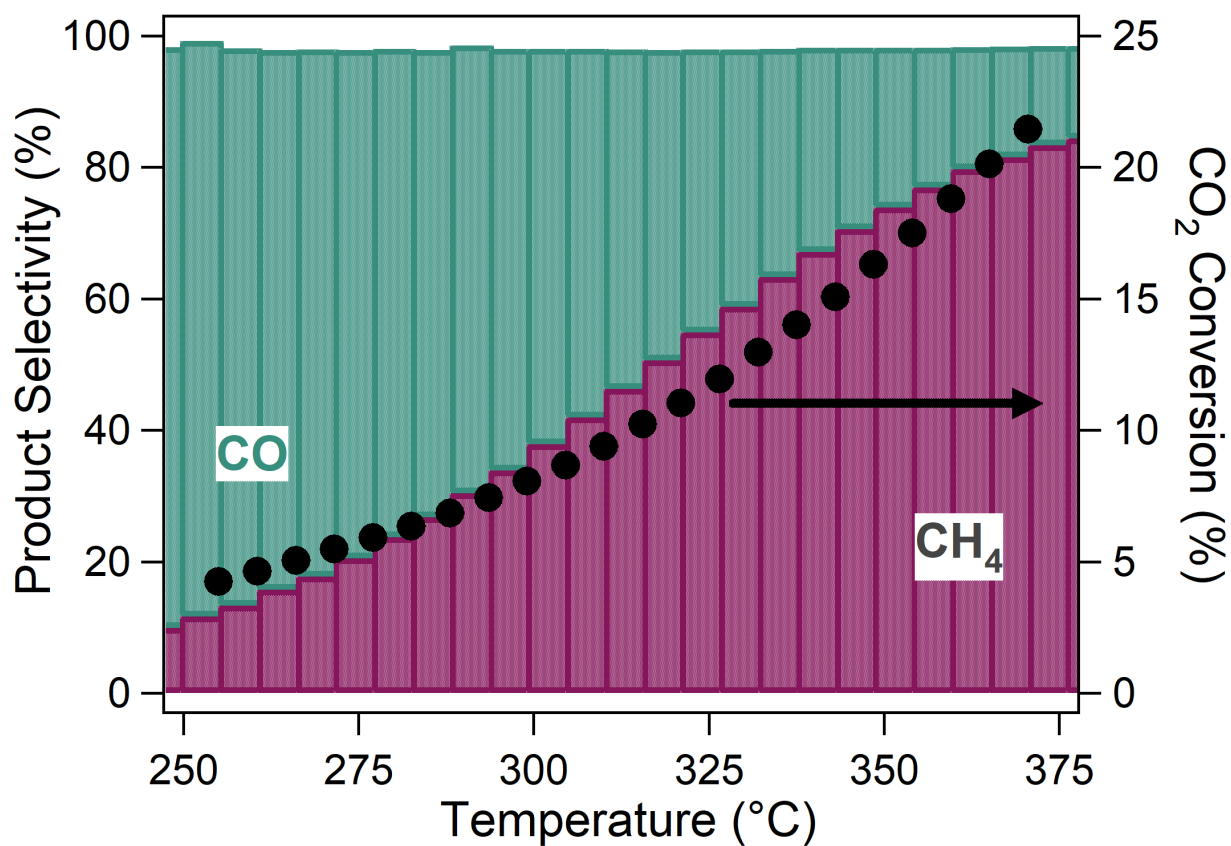


Figure B.23: Reverse water-gas shift performance of 1Ni-WC(900). The reaction temperature is ramped at a rate of 0.25 °C/min at a gas hourly space velocity of 27,000 mL/h/gcat with a 3:1 H₂:CO₂ reactant ratio at 2.1 MPa.

B.2 In-House Reaction Dataset

Table B.2: CO Yield Dataset for Reverse-Water-Gas-Shift Reaction Inverse Catalyst Design

Tungsten Loading (wt%)	Dopant	Dopant (wt.%)	Carburization Temp (°C)	Reaction Temperature (°C)	CO yield (%)
15	Fe	0.5	835	280	1.66
15	Fe	0.5	835	350	3.03
15	Fe	5	835	280	1.61
15	Fe	5	835	350	4.12
15	Cu	0.5	835	280	0.52
15	Cu	0.5	835	350	3.36
15	Cu	5	835	280	9.80
15	Cu	5	835	350	18.98
15	Co	0.5	835	280	6.21
15	Co	0.5	835	350	16.35
15	Co	5	835	280	1.73
15	Co	5	835	350	2.85
4.25	–	–	600	350	2.23
4.25	–	–	835	350	5.14
4.25	–	–	1000	350	4.63
15	–	–	600	350	5.72
15	–	–	835	350	8.73
15	–	–	1000	350	5.09
15	Pt	0.5	835	280	2.32
15	Pt	0.5	835	350	7.59
15	Ni	0.5	835	280	2.67
15	Ni	0.5	835	350	7.85
15	Ni	0.25	835	350	9.54
15	Cu	0.25	835	350	4.55
15	Co	0.25	835	350	5.66
15	Fe	0.25	835	350	0.78
15	–	–	680	280	1.47
15	–	–	680	350	10.43
15	–	–	600	350	5.72
15	–	–	835	350	8.73
15	–	–	1000	350	5.09
15	–	–	600	350	5.72
15	–	–	700	350	6.79
15	–	–	800	350	6.87
30	–	–	600	350	7.24
30	–	–	700	350	10.38
30	–	–	800	350	10.89

B.3 MaxMarginalRelevance vs SemanticSimilarity (Context Selection Methods)

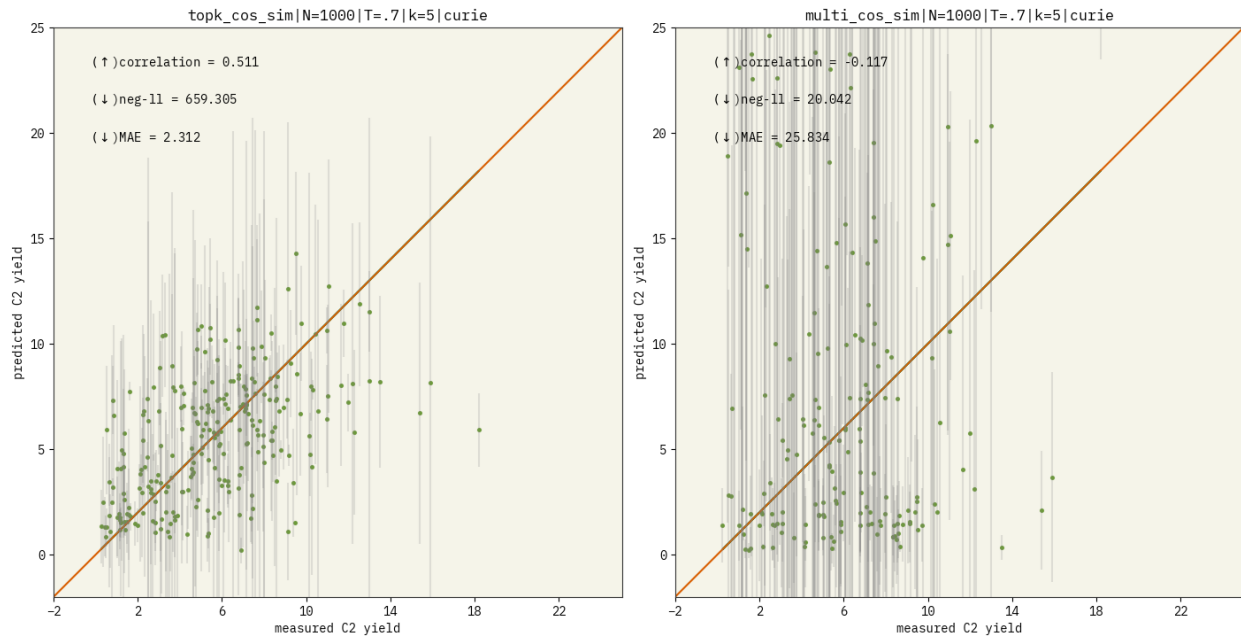


Figure B.24: These are the results of applying topk and multi using the SemanticSimilarity (SS) function from Langchain as opposed to our selected approach of using MMR for context selection. SS uses cosine similarity to select the next context point, whereas MMR offers a more diverse selection of context for robustness. This figure elucidates the importance of distinct context for ICL. These results may be compared to the other regression figures that used the MMR in the rest of the experiments.